AN ABSTRACT OF THE THESIS OF

Kyle James Maloy for the degree of Master of Science in Radiation Health Physics presented on May 18, 2006.
Title: Radiation Health and Safety of a Radioisotope Powered Micro Fuel Cell.

Redacted for Privacy

Abstract approved:

Dr. Todd Palmer

Radiation health and safety issues associated with a plutonium-powered radioisotope powered micro fuel cell (RMFC) were evaluated. The RMFC converts water into its component elements by radiolysis and the resultant hydrogen is used to power the fuel cell. This device is under development and is being considered for possible deployment with unattended sensing devices. In addition to emitting alpha particles from the decay of plutonium, the RMFC produces secondary neutrons via (α,n) reactions. Several exposure scenarios were examined in order to assess the potential radiological impact from an intact, and a breached device. The scenarios include dose to personnel 30 cm from an RMFC, implanting a device in the chest cavity, and accidentally ingesting a device. All exposure scenarios with the intact RMFC resulted in total effective dose equivalent rates of less than 2.5 rem per year. Exposure scenarios with a damaged RMFC considered inhalation of the radioisotope and resultant dose at acute (1-day) and committed (50-year) time frames. Inhalation dose coefficients (Sv/Bq) from Federal Guidance Report 11 were used to determine the resultant committed effective dose equivalent (CEDE) and relative risk due to the

inhalation of the radionuclide. NUREG/CR-4214 guidelines for deterministic effects of acute exposure were used to examine the risk and possible lethality from high dose-rate acute exposures. These exposure scenarios were considered conservative, because no mitigating features were incorporated into the design of the RMFC. Mitigating features can reduce the amount of neutrons from (α,n) reactions and limit the amount of the radioisotope that will be available for atmospheric dispersion in the event the device is breached. The final analysis concludes that the dose to individuals living in a zone where the device has been breached will not exceed 60 mrem in any one year following a dispersion event.

Although the RMFC is not necessarily designed to operate under the proposed exposure scenarios, a comprehensive evaluation of possible modes of exposure is informative and prudent This is particularly true because the device employs radioactive material, and applications of this technology demand the highest rigor in evaluating any plausible normal operation, or accident exposure scenario. This analysis will aid in the ongoing development of the RMFC prototype.

Radiation Health and Safety of a Radioisotope Powered Micro Fuel Cell

by
Kyle James Maloy

A THESIS

submitted to

Oregon State University

in partial fulfillment of
the requirements for the
degree of

Master of Science

Presented May 18, 2006
Commencement June 2006

Master of Science thesis of Kyle James Maloy
presented on May 18, 2006.

APPROVED: Redacted for Privacy

Major Professor, Representing the Department of Nuclear Engineering and Radiation Health Physics

Redacted for Privacy

Head of Nuclear Engineering and Radiation Health Physics

Redacted for Privacy

Dean of the Graduate School

I understand that my thesis will become part of the permanent collection of Oregon State University libraries. My signature below authorizes release of my thesis to any reader upon request.

Redacted for Privacy

Kyle James Maloy, Author

TABLE OF CONTENTS

TABLE OF CONTENTS (Continued).

LIST OF FIGURES

LIST OF TABLES

LIST OF TABLES (Continued).

RADIATION HEALTH AND SAFETY OF A
RADIOISOTOPE POWERED MICRO FUEL CELL

1. INTRODUCTION

The technological advancements accomplished in the 20th century will be improved upon in the next century. Products being developed are lighter, smaller and more efficient. Micro electro mechanical systems (MEMS) are an example of such technology. Common MEMS applications are accelerometers used in airbag deployment, pressure sensors for tires, and gyroscopes used to indicate and stabilize yaw for automobiles and aircraft (Madni and Wan, 1998).

The enhancement of power-sources for MEMS has the potential to increase the lifetime and the utility of these micro-systems. Current chemical battery technology does not have sufficient lifetime or suitable mass-power density ratio to serve as a MEMS device integrated power source (DARPA, 2004). A power source that has a substantially longer life than a chemical battery and that is contained in a smaller volume will allow MEMS technologies to operate as dispersed, unattended actuators and remote sensing equipment independent of larger systems. There are at least ten universities and numerous private firms engaged in the research and development of micro-gas turbines, micro-combustors, and micro-rotary engines with the hope of harnessing mechanical or electrical power from these devices (Berkeley, 2006; Green, et al, 2004; Kathiolieke, 2006; MIT, 2006; MDOT, 2006; Univ. of Birmingham, 2006; Univ. of Minnesota, 2006; Walther and Pisano, 2003; WSU, 2006; Whalen, et al,

2003). The power density and life of these devices are potential advantages over conventional battery technology, but they all require an external source of hydrocarbon fuel to operate.

Small scale power generation using radioisotopes has the potential to power remote sensors or actuators for years without significant power loss. Radioisotope thermal generators (RTGs) have been used by NASA to power space probes and manned vehicles in notable space programs such as Apollo and Cassini (Furlong and Wahlquist, 2003). The radioisotope ^{238}Pu has also been used to power pacemakers that stimulate a regular heartbeat when the body's natural 'pacemaker' is not working correctly (ORAU, 2006). Approximately 250 plutonium powered pacemakers were manufactured in the 1970s, and between 25 and 50 of the hearts of these recipients were still beating regularly in 2003 (ORAU, 2006).

A new technology is being developed that intends to employ an α-emitting radionuclide to supply hydrogen to a tiny fuel cell. The fuel cell will utilize the hydrogen to generate an electric current. A radioisotope-powered micro fuel cell (RMFC) would have power output proportional to the activity of the radioisotope. The proposed design of an RMFC would be contained in a volume of 1 to 2 cubic centimeters and would be capable of sustained power generation of 10 mW for years. An RMFC which would continue to generate power with losses due to radioactive decay not exceeding 3% per year would be applicable to the areas of dispersible unattended sensors, munition storage, mission-critical battery applications, actuators, and emergency beacon deployment and use (DARPA, 2004). ^{238}Pu is an α-emitter

that experiences loses less than 1% of its activity per year, and is the radioisotope of primary interest at this time (Misner, 2005).

The operating basis for the device is to use radioactive decay products (5.5 MeV α's from ^{238}Pu) to dissociate water into H_2 and O_2. A small fuel cell would use the resulting molecular hydrogen and oxygen (liberated as a result of radiolysis) to generate power output in the 10 mW power range. A conventional fuel cell requires an external source of hydrogen and oxygen as fuel. The proposed RMFC would generate its own H_2 and O_2, which would then recombine at the electrodes of the fuel cell to generate power and water. The RMFC would be regenerative and have no emissions. The reactions which take place to produce power are the oxidation of hydrogen at the anode and the reduction of oxygen at the cathode:

Anode (H_2 oxidation) $2H_2 + 4OH^- \Rightarrow 4H_2O + 4e^-$ **(1.1)**

Cathode (O_2 reduction) $4e^- + 2H_2O + O_2 \Rightarrow 4OH^-$ **(1.2)**

Overall Reaction $2H_2 + O_2 \Rightarrow 2H_2O$ + energy **(1.3)**

The radiation health and safety concerns of the RMFC need to be considered in order to determine the feasibility of the possible operating modes of such a device. The analysis of plausible scenarios which would expose persons to radiation from an intact RMFC or to the radioactive source material contained therein, will aid in deciding how such a device will be used.

The safety of an RMFC that is wholly intact and uncompromised was considered from multiple perspectives. The α or β dose from an intact RMFC is

virtually non-existent because the α and β particles deposit all their energy inside the device. However, there is potential cause for concern because (α,n) reactions with naturally occurring trace isotopes of oxygen[1] (^{17}O, ^{18}O) in H_2O, and oxides such as PuO_2 or Gd_2O_3, produce neutrons which do travel beyond the bounds of the fuel cell. The scenarios considered in this assessment examined a fully intact RMFC: 1) placed permanently in the body (analogous to a pacemaker, nerve stimulator, or circulatory assist system); 2) ingested by an individual, consequent travel through, and resultant dose to the GI tract; and 3) exposure to the RMFC dose rate at a distance of 30 cm^2.

In order to analyze the scenarios described in 1-4 above, the radiation transport code Monte Carlo-N-Particle X (MCNPX) was used to transport the α-particles through the device. Monte Carlo-N-Particle Version 5 (MCNP5) was used to calculate the dose from the secondary neutrons produced. Because the cost, availability, and safety concerns associated with the radioisotope of interest are significant, measurements using real radionuclides were not pursued. The MCNP family of codes is available at Oregon State University to licensed users. MCNP is considered accurate and accredited by those in the nuclear engineering and health physics professions.

Additional scenarios of concern involve an RMFC that has been compromised and is no longer fully intact. As a consequence, the PuO_2 source material will no longer be encapsulated, and may come in direct contact with the environs. If the

---

[1] Natural oxygen has three naturally occurring isotopes, ^{16}O—99.757%, ^{17}O—0.038%, ^{18}O—0.205%

[2] As per RMFC project goals outlined in the proposal, the dose rate 30 cm from the device shall not exceed 1000 mrem/yr (DARPA,2004).

source is in a nano-particle suspension or slurry, a large fraction of the material will be respirable and transferable to the blood where it will be systemically distributed.

The computer code HOTSPOT was used to simulate the scenario of source material being 'exploded' at a low altitude. The resultant dispersed material that could possibly be inhaled was evaluated. Various atmospheric stability conditions and wind speeds were considered for plume dispersal.

To determine the environmental transport of radioactive material released from an RMFC that has been breached, the RESRAD computer code was used.

The remainder of this thesis is organized in the following way. Chapter 2 contains a review of relevant literature and motivation for this research. Chapter 3 provides the methods and, where necessary, explanation of the computer codes used in the calculation of results. The results of the calculations and simulations performed for each scenario and respective discussion are presented in Chapter 4. Chapter 5 contains a conclusive summary of the work completed in this analysis and suggestions for future research.

2. LITERATURE REVIEW

2.1 Hydrogen Generation from Breached Spent Fuel.

A fully operational RMFC will internally produce hydrogen through radiolysis of water. Previous work on the topic of hydrogen generation via radiolysis was completed in 2002 by the Westinghouse Savannah River Company in Aiken, SC. The work is titled "Evaluation of Hydrogen Generation from Radiolysis from Breached Spent Fuel" (Vinson, et al, 2002). The motivation for the work was to qualitatively determine if physical conditions permit the buildup of hydrogen gas inside the water filled shipping casks at the Savannah River Site.

Hydrogen production by way of radiolysis was examined. It was determined that high LET radiation, (α-particles, for example) is effective at decomposing water into its component elements which may recombine to produce both molecular and ionic species under the following reaction in Equation 2.1 (Vinson, et al, 2002):

$$H_2O \xrightarrow{\text{incident radiation}} H_3O^+_{aq},\ OH,\ e^-_{aq},\ H,\ H_2O_2,\ H_2 \qquad \textbf{(2.1)}$$

The presence of β or γ radiation increases the rate of the reverse reaction, shown below in Equation 2.2 (Vinson, et al, 2002):

$$\frac{H + H_2O_2 \rightarrow OH + H_2O}{OH + H_2 \rightarrow H + H_2O} \quad net: H_2 + H_2O_2 \rightarrow 2H_2O \qquad \textbf{(2.2)}$$

The reverse reaction causes the chemical species produced by the process of radiolysis to recombine and produce water. The reverse reaction is beneficial in the

case of spent fuel storage because it limits the evolution of large quantities of flammable hydrogen gas in the air space of the storage casks (Vinson, et al, 2002).

The Westinghouse study asserted that hydrogen production is linearly proportional to the energy density of the α-radiation in the aqueous solution. This study confirmed that α-radiation is the most productive means of radiolytic hydrogen generation, and the addition of γ or β sources only hinders the hydrogen evolution. In Vinson's work, evolution of hydrogen was undesirable and was observed to level off once the concentration of dissociated hydrogen reached a certain point[3]. The reverse reaction then begins working against the forward reaction (Equation 2.1) and an equilibrium concentration is reached. In the RMFC the hydrogen will be consumed at the fuel cell anode surface. It is hypothesized that the rate of the reverse reaction will be minimized because the fuel cell will convert the hydrogen back to water.

2.2 Radiolysis of Water Using Plutonium Oxide

There is an optimal design of the RMFC that maximizes radiolytic hydrogen production but keeps the amount of source material to a minimum. The variation of particle size and amount of water is shown to have a noticeable effect on hydrogen generation rates. Work was published in Russia in 2002 (Vladimirova and Kulikov, 2002) that quantifies the influence of source particle size and concentration of H_2O about the source on source effectiveness. The work was completed at the Bochvar

[3] The point referred to is when the forward and reverse reactions reach equilibrium. The 'leveling off' is dependent on the rate of the forward reaction and thus the radiolytic H_2 production.

Russian Research Institute of Inorganic Materials under the State Scientific Center of the Russian Federation. The title of the work is, "*Formation of H_2 and O_2 in Radiolysis of Water Sorbed on PuO_2*" (Vladimirova and Kulikov, 2002).

The purpose of Vladimirova and Kulikov's 2002 work was to determine the effect of % water sorbed in two varieties of PuO_2 on the evolution of hydrogen gas. Vladimirova and Kulikov (2002) used PuO_2 of reactor quality[4] that was categorized as either high-burn-up (h.b.) or low-burn-up (l.b.) variety[5]. The % water sorbed on the PuO_2 was 0.3, 1.0, 1.5, 2.0, or 3.0. (See Table 2.2)

Table 2.2 Rates and radiation chemical yields of H_2 and O_2 for various samples of PuO_2 (Vladimirova and Kulikov, 2002)

Type of PuO_2 Sample	H_2O content %	Rate cm^3 (g $PuO_2)^{-1}$ day^{-1}		Yield molecules per 100 eV	
		V_{H_2}	V_{O_2}	G_{H_2}	G_{O_2}
		High-burn-up plutonium			
Pellet	0.3	0.01	0.001	1.1	0.10
"	1.0	0.07	0.01	2.4	0.35
"	1.5	0.16	0.025	3.65	0.57
"	2.0	0.29	0.04	5.0	0.7
"	3.0	0.6	0.1	6.9	1.1
Powder	3.0	0.75	0.08	8.6	0.92
		Low-burn-up plutonium			
Powder	3.0	0.12	0.015	8.5	1.1

The quantitative results of the work were that increasing of the percentage of water sorbed on the PuO_2 by a factor of 10 (from 0.3% to 3.0%) increased the volume of gaseous hydrogen and oxygen produced via radiolysis by a factor of 60 and 100, respectively (Vladimirova and Kulikov, 2002).

---

[4]. wt%: ^{238}Pu 0.5-0.6, ^{239}Pu 65-67, ^{240}Pu 21.7-22.7, ^{241}Pu 7.7-8.1, ^{242}Pu 2.5-2.9.

[5] h.b. had α-activity of 0.3 $Ci \cdot g^{-1}$ while l.b. had α-activity of 0.0625 $Ci \cdot g^{-1}$.

The primary conclusion of their research was that the evolution of hydrogen and oxygen gas by way of radiolysis had a substantially high G value (or radiation chemical yield[6]) when water is sorbed on the PuO_2. This is in contrast to PuO_2 that was suspended in an aqueous slurry or mixture. Smaller particle sizes (of the PuO_2) also increased the rate of radiolysis of the water. Small particle size and sorbed water (as opposed to 'free' water) ensure more of the α energy is deposited in the water. Consequently, there is less opportunity for recombination of products if the volume of water does not completely surround the plutonium oxide.

2.3 Neutron Energy Spectra of $^{238}PuO_2$ from O(α,n)Ne Reactions

The secondary neutrons being produced in the RMFC will travel beyond the material encapsulating the device. It is important to know the energy distribution of neutrons from this source in order to accurately model its dosimetry.

M.E. Anderson (1980 and 1985) has conducted two experiments and published two papers that report the neutron energy spectra of two plutonium oxide sources. The 1980 work was being carried out in order to subsequently develop accurate personnel neutron dosimeters for use in PuO_2 processing plants and other environments where neutrons are of concern.

The sample of PuO_2 used in Anderson's 1980 analysis contained 1.19 g of ^{238}Pu and weight fractions of isotopes of plutonium were ^{238}Pu—0.8, ^{239}Pu—0.16,

[6] Radiation chemical yield is defined as the number of molecules produced in a given medium per energy deposited in that medium, i.e., molecules H_2 per 100 eV energy deposited in that medium.

^{240}Pu—0.03, ^{241}Pu—0.01. Approximately 99.9% of the α activity in this source is attributable to ^{238}Pu. The sample was enriched in trace isotopes of ^{17}O and ^{18}O, yielding a higher neutron source strength than 'natural oxygen' plutonium oxide[7]. Although the isotopic abundances of trace isotopes of oxygen are greater in the enriched oxide, the energy spectrum of the neutrons produced should be the same as natural (oxygen) PuO_2.

The neutron yield and energy spectrum from the PuO_2 source was determined with the use of a precision long counter and a liquid scintillation fast-neutron spectrometer. The long counter and scintillation spectrometer were then used with the unmoderated source and with the source being consequently placed inside polyethylene spheres of 7.6 cm, 12.7 cm, 20.3 cm, 25.4 cm, and 30.5 cm (Anderson, 1980).

Anderson also reported the neutron energy spectrum from a plutonium source that was employed to supply heat for a radioisotope thermal generator (RTG) for use in space applications (Anderson, 1985). The source was 10 kg of plutonium and contained a mixture of plutonium isotopes: (mass percentages) 83.6 % ^{238}Pu, 14.0 %^{239}Pu, 2.0 % ^{240}Pu, 0.4 % ^{241}Pu, and 0.1 % ^{242}Pu. Anderson's 1985 method of determining the neutron energy spectrum from this source was nearly identical to the method in his previous work (Anderson, 1980; Anderson, 1985). The spectra of the 1.19 g and 10 kg sources are shown below in Figure 2.3.

---

[7] Oxygen isotopes occur in nature as 0.99757 ^{16}O, 0.0038 ^{17}O, and 0.00205 ^{18}O. Anderson's sample contained 0.68 ^{16}O, 0.01 ^{17}O, 0.31 ^{18}O.

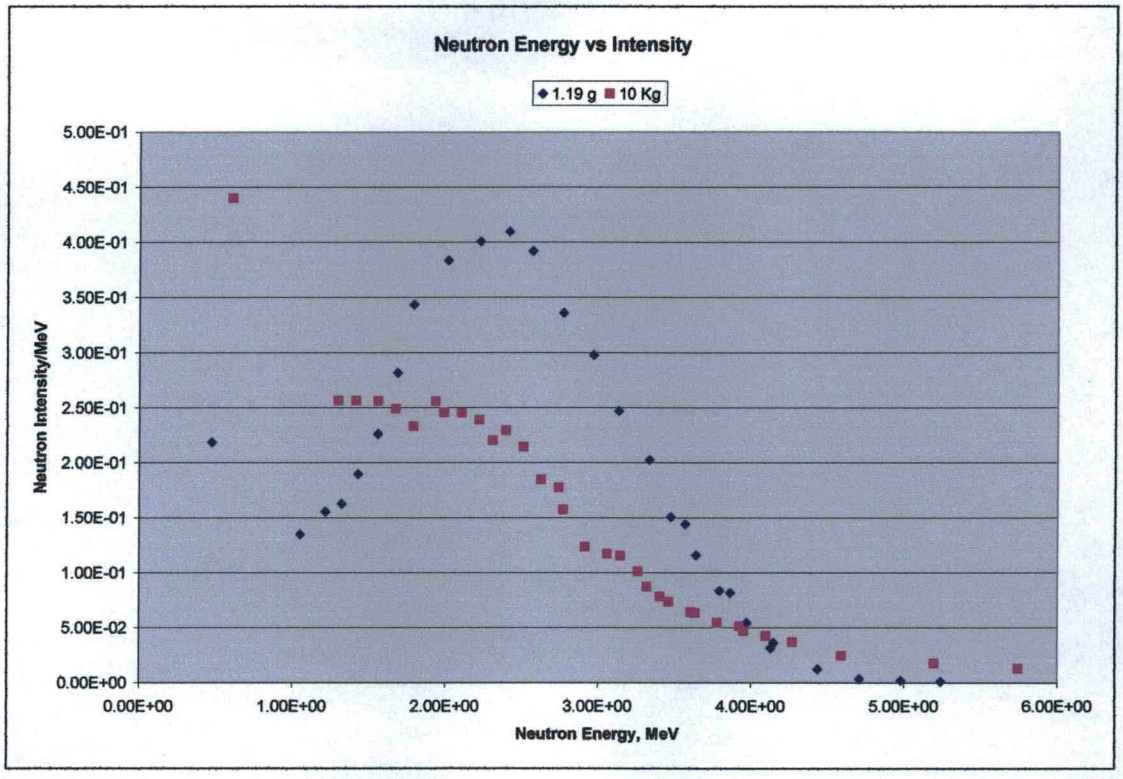

Figure 2.3 Neutron energy spectrum of 1.19 g and 10 kg sample of PuO_2 (Anderson, 1980 & 1985)

In Figure 2.3, neutrons with energies below 1 MeV are assigned energy of 0.5 MeV. The neutron liquid scintillator only has a reliable counting efficiency for neutrons above 1 MeV (Anderson, 1980). In contrast, the long counter has a relatively flat response for neutrons with energies between 2 keV to 6 MeV (Knoll, 1999). Hence, below 1 MeV, the difference between the integrated neutron spectrum obtained from the liquid scintillation spectrometer and the number of counts from the long counter is assigned a value of 0.5 MeV. Observation of dose conversion factors for neutrons from ICRP-21 (1971) shows that for neutrons with energies between 0.025 eV and 1 MeV, neutrons with energy of 0.5 MeV have the highest flux to dose rate. This maximizes the dose contribution calculated from low energy neutrons using these

spectra. The precise magnitude of the effect is unknown but expected to be less than 10% and keeps dose calculations conservative.

2.4 Survey of Emerging Power MEMS Technology

In a brief overview of emerging power sources for use with MEMS technology, Jacobson and Epstein (2003) summarize various modes and applications of power sources for MEMS devices. Micro-fuel cells are only briefly mentioned and the major focus is given to small combustion engines that perform mechanical work such as fluid pumping or propulsion and, in some cases, generate electric power. Some attention is also devoted to direct electrical conversion devices such as heat scavengers which produce electricity by thermoelectric means via a temperature gradient across the device.

Research and development of MEMS power sources is currently being conducted at Oregon State University (DARPA, 2004), UC Berkley (Berkley, 2006), MIT (MIT, 2006), Washington State University (WSU, 2006), the University of Tokyo and Stanford University (Jacobson and Epstein, 2003). The power sources being developed produce power in the 1-50 W range with the intent of powering personal electronics devices, first for military applications and then, possibly at the consumer level. The authors also note devices which produce power in the milli-Watt range for remote sensing equipment and actuators (Jacobson and Epstein, 2003).

The authors list the challenges encountered by the small,-high power density devices. The micro-combustion engines under development will operate at high

frequencies and under considerable strain, requiring meticulous materials selection and manufacturing of components. As Jacobson and Epstein (2003) point out, conventional size piston engines already operate with clearance tolerances at the micron level, which implies micro-combustion engines must meet even more strict tolerance standards, or employ alternative features less sensitive to these constraints..

Heat engines that operate on the premise of temperature differences and that employ thermoelectric generators to generate an electric current, run into challenges at the micro-scale. The cold and hot side of the devices must be thermally isolated, which would seem to prove extremely difficult in micro-scaled devices.

The RMFC has no moving parts, nor does it require a temperature gradient to produce power.

2.5 Standards for Prosthetic Devices Containing Radionuclide Power Sources

Smith (1971) outlined proposed medical devices that could have their lifetime significantly increased if they were to employ a radioisotope as their power source (Smith, 1971).

At the time of the publication, a typical heart pacemaker could run for up to two years on mercury batteries. The 'nuclear battery' had an expected lifetime of ten years (Smith, 1971).

The benefits of using nuclear technology to lengthen the operating life and power density of such devices as pacemakers, nerve stimulators, and circulatory assist systems are readily apparent. When developing and employing new technologies it is

important to evaluate their potential risks. It is necessary to evaluate the risks and safety concerns while a technology is being developed, rather than while in post-development and production phases. Accident mitigation and preventative measures can be incorporated into the development of devices, which would otherwise halt the development and manufacture of such appliances.

This review of small nuclear powered devices and the need for safety standards is just as prudent to the development of a radio-isotope powered fuel cell as it was to medical devices that were being designed and envisioned in the 1970s.

3. METHODS

3.1 Monte Carlo Method, MCNP5 and MCNPX

The Monte Carlo technique can be used to model a physical process using probability distribution functions and random number generators. With the use of the Monte Carlo technique, it is possible to model the interactions in the life of a particle from its birth to its death. The interaction of radiation with matter is a stochastic process. Monte Carlo radiation transport codes sample probability distributions and transport particles based on interaction probabilities using a random number generator to compile a specified number of particle histories. These histories are used to generate statistically robust results that characterize a user-defined physical situation.

The Monte Carlo computer code MCNPX (Waters, 2002) was used to determine the neutron source strength as a result of the $^{17}O(\alpha,n)^{20}Ne$ and $^{18}O(\alpha,n)Ne^{21}$ reactions. This neutron source strength and neutron energy spectrum were used as input to MCNP5 (Briesmeister, 1993) to carry out neutron dose calculations.

The Monte Carlo codes MCNPX (Waters, 2002) and MCNP5 (Briesmeister, 2002) require:

- Geometry specification of the problem in three dimensions;
- Isotopic composition of materials and cross sections;
- Source information (strength, energy, location, direction); and
- Tally specification.

A detailed explanation of problem-specific, user-defined inputs is included in the following sections.

3.2 Neutron Source

To determine the neutron source strength resulting from (α,n) reactions with heavy-trace isotopes of oxygen, the MCNPX code was used. Unlike MCNP5, MCNPX is able to transport α-particles. It has been previously determined (Misner, 2005) that the required mass of ^{238}Pu necessary to generate the needed amounts of H_2 and O_2 for a 10 mW power output is ≈ 1 g. The activity of 1 gram of ^{238}Pu is slightly greater than 17 Ci. Fortunately, from a radiation dose standpoint the α-particles emitted by the ^{238}Pu nucleus have a range in the RMFC of about 40 μm. However, because the plutonium to be employed for use in the fuel cell is in an oxide form (PuO_2), the O(α,n)Ne reactions are of concern. A mass of 1.13 grams of $^{238}PuO_2$ contains an equal amount of ^{238}Pu atoms as a gram of the isotope in pure form, and as a direct result, equal activity. So, the required mass of the oxide form is 1.13 grams to produce the required continuous power output of 10 mW.

With the PuO_2 having a density of 11.64 g/cm^3, the corresponding volume of 1.13 g of the PuO_2 is 0.098 cm^3. A sphere with this volume was defined in MCNPX (radius 0.286 cm). The source was defined to have an activity of 6.3E11 disintegrations per second (17 Ci) and to be distributed uniformly throughout the sphere.

To determine the neutron source strength (neutron·s^{-1}) a volumetric flux (F4)[8] tally was used in the PuO_2 cell. The macroscopic cross sections ($\Sigma_{\alpha,n}$) for $^{18}O(\alpha,n)^{21}Ne$ and $^{17}O(\alpha,n)^{20}Ne$ reactions were calculated using the microscopic reaction cross sections (Vukolov, 1983) and atom densities of the oxygen isotopes[9]. An Excel spreadsheet was used to repeat the calculation to determine energy dependent macroscopic cross sections for input on the DF card of MCNPX for each corresponding DE (energy) card. The product of the F4 α flux tally and the energy dependent (α,n) reaction cross sections allows MCNPX to calculate the neutron source strength, using Equation 3.2.

$$\text{Reaction Rate: } N\int \sigma_{\alpha,n}(E)\,\phi(E)\,dE \left(\frac{atom}{cm^3}\right)\left(\frac{n\cdot cm^2}{\alpha\cdot atom}\right)\left(\frac{\alpha}{cm^2\cdot s}\right)=\left(\frac{n}{cm^3\cdot s}\right) \qquad \textbf{(3.2)}$$

The scenario explained above was used to calculate the neutron source strength resulting from α's colliding with the heavy isotopes of oxygen in the oxide fuel. Because the amount of ^{238}Pu needed to generate enough H_2 and O_2 for 10 mW power output was determined by calculating the energy deposited in water to generate the radiolysis products for the fuel cell, a second scenario was considered to determine the neutron source strength when all the energy of the α-particles was deposited in H_2O rather than the PuO_2.

[8] An F4 tally returns the value of average flux in a user defined cell.
[9] $\Sigma = N\sigma$.

3.3 Neutron Dose to Personnel @ 30 cm

Once the neutron source strength was determined, MCNP5 was used to transport the neutrons and calculate the neutron dose rate. The geometry of the source remained the same as in the MCNPX model, a sphere 0.286 cm in radius, but the source particles transported were neutrons and not α particles.

The source was surrounded by 1/2" (1.27 cm) of steel. A spherical surface is defined 30 cm from the outer edge of the steel capsule as per requirements for RMFC project goals, and a surface flux (F2) tally is defined on this surface to calculate the average neutron flux ($n \cdot cm^{-2} \cdot s^{-1}$). The material between the tally surface and the source material is defined to be air[10]. The F2 surface flux tally was modified by ICRP-21 neutron flux-to-dose-rate conversion factors $\left(\frac{rem/hr}{n/cm^2 \cdot s}\right)$. The conversion factors are used in the code, so that neutrons of different energies which reach the tally surface are scored according to their energy and corresponding conversion factor. MCNP interpolates the flux-to-dose conversion factor for neutrons with energy lying between two defined dose conversion factors recorded on the tally surface.

The energy spectrum of the source neutrons is specified by the user. Initially, a mono-energetic source was assumed with the neutron energy set at 5.5 MeV. Subsequently, literature was located which detailed experimentally measured energy spectra of neutrons born of (α,n) reactions in PuO_2 (Anderson, 1980; Anderson, 1985) and uranium/plutonium oxide fuel pins (Babut, 2004).

---

[10] Material 'air' defined as 0.8 nitrogen and 0.2 oxygen by mass fraction with a density of $0.00129 g/cm^3$

3.4 MIRD Phantom

To calculate the dose to internal organs via a specified ingestion or implantation of an RMFC, a computational model of a human torso phantom was constructed. The phantom was constructed using guidelines outlined by the Society of Nuclear Medicine's Medical Internal Radiation Dose Committee (Snyder, 1969). The phantom will hereafter be referred to as the modified MIRD phantom. The literature (Snyder, 1969) specifies the shape, location, and volume of each of the organs. The organs used in the model are the stomach, small intestine, upper large intestine, colon, heart, left kidney, liver, left lung, left ovary, pancreas, spleen, left testicle, thymus, thyroid, uterus, left adrenal, and the urinary bladder.

To facilitate MCNP5 simulation, modifications of the MIRD phantom were necessary for the colon, heart, thyroid, uterus, and urinary bladder. The changes were either in (x, y, z coordinate) position of the organ within the body, or simplifications in the specified geometrical shape of the organs. The volumes of all organs were maintained as specified in the MIRD phantom (Snyder,1969).

In the MIRD phantom model, the colon is s-shaped and wraps behind the uterus and over the urinary bladder. In the modified MIRD phantom the colon was defined as a straight cylinder with its horizontal extent remaining identical to that specified in the MIRD phantom (Snyder, 1969). In its new configuration, the colon overlapped the uterus and urinary bladder. As a result, the bladder was moved down 3.4 cm while the uterus was moved down 4 cm and shifted 2.5 cm in a dorsal manner.

The MIRD phantom model called for the heart to be constructed of two portions: a partial-ellipsoid, capped by a hemisphere. The heart's specified volume and physical location within the constructed phantom were maintained, however the heart was treated as a sphere. Lastly, the geometry of the thyroid was modified so that the two lobes were condensed, while the volume and surface area of the organ were maintained.

From a radiation dose standpoint, the modifications made to the MIRD phantom should still provide reliable dose measurement estimates for this portion of the analysis. To obtain a more accurate dose to a particular person, the specific individual would need to be modeled. Small modifications should not significantly affect the model's ability to estimate dose to a typical individual from the general population.

A three dimensional representation of the modified MIRD phantom is shown in Figure 3.4a and 3.4b. The transverse upper large intestine is not visible in either of the figures but is present inside the volume of the small intestine. It is represented as an elliptical cylinder located at the top of the small intestine area, with horizontal extent just less than that of the small intestine and respective major and minor radii of 2.5 cm and 1.5 cm as specified in the MIRD model (Snyder, 1969).

Only the left organs were modeled for those that occur in pairs (lung, gonad, kidney, and adrenal). The implanted device simulation was oriented on the left side of the body. The source placement for the digestion model keeps the source on the centerline of the body in the small intestine, large intestine, and colon. The stomach is

on left side of the body. It was assumed that by only modeling the organs on the left side of the body it would decrease the time for the MCNP simulations to run. Furthermore the dose calculation will remain conservative for these organs as long as the source orientation is to the left of the phantom's centerline.

The RMFC was placed in the chest cavity to simulate implantation of the RMFC, and the results of the transport calculation can be seen in Table 4.3a. The RMFC was also placed in the stomach, small intestine, large intestine, and colon for respective times of 1, 4, 13, and 24 hours. These times correspond to the ICRP-30 (1974) gastrointestinal tract model transit time for digestion. See Table 4.3b for digestion dose results.

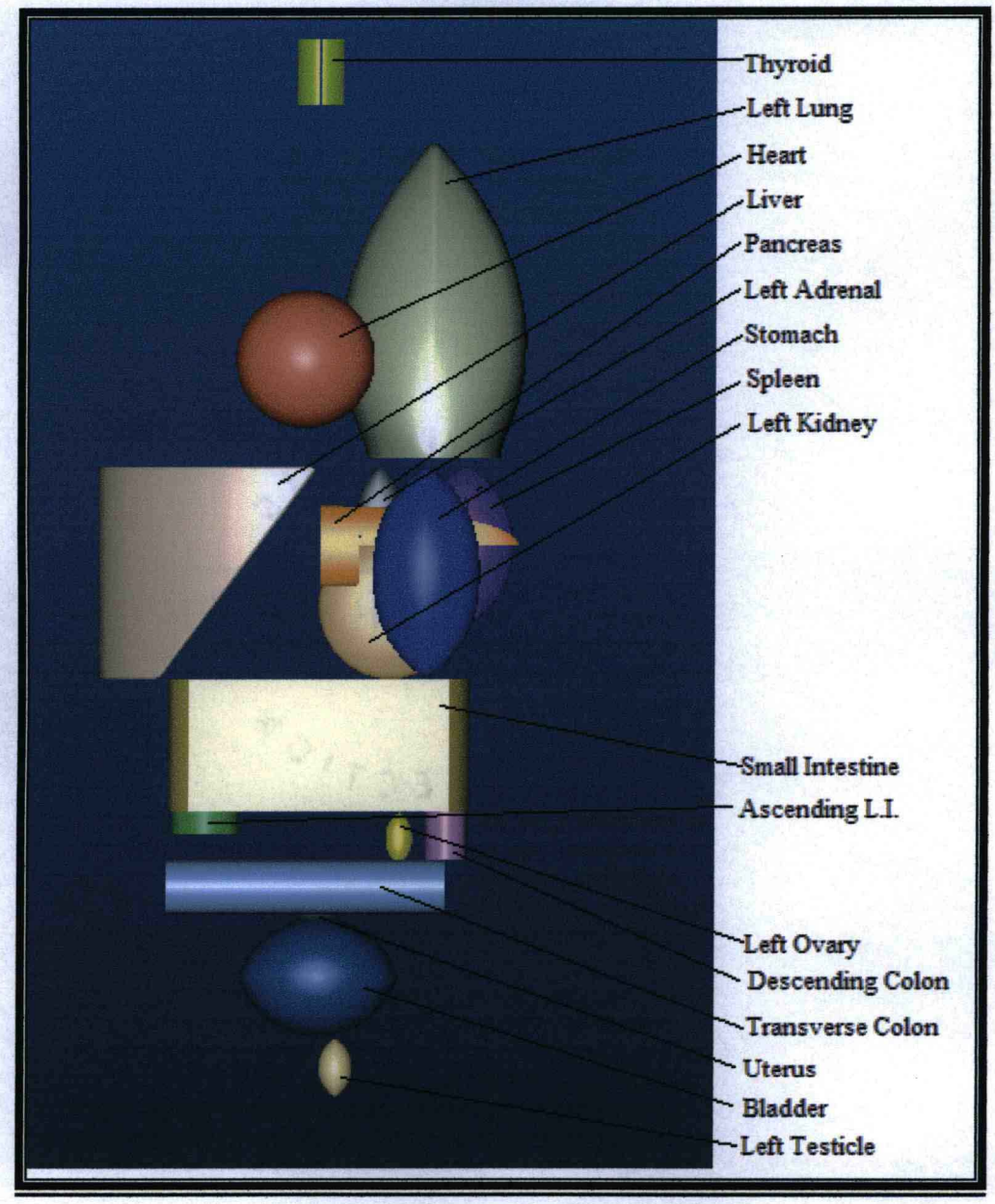

Figure 3.4a Modified MIRD phantom organs (front view)

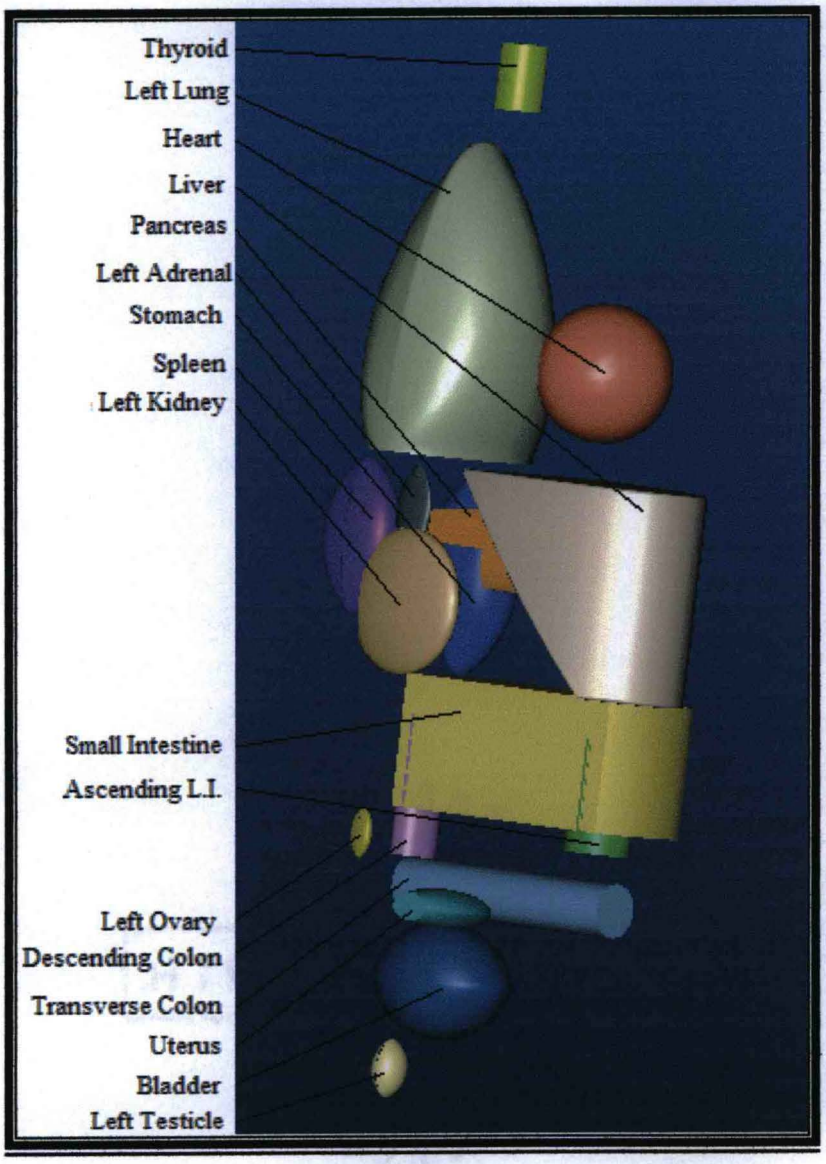

Figure 3.4b Modified MIRD phantom organs (dorsal view)

3.5 Neutron Dose Through Tissue

To determine the dose to the body resulting from a generic ingestion, implantation, or wearing or holding the device on the surface of the body, the dimensions of the source were maintained as a sphere of PuO_2 with radius 0.286 cm and density 11.64 g/cm^3. The neutron energy spectrum selected was that of the 1.19 g sample of plutonium oxide (Anderson, 1980). In order to keep the volume of the modeled RMFC at 1 cm^3 the thickness of steel chosen to encapsulate the source material for this simulation was ≈ 1/8" (0.33 cm)[11].

The ICRU reference sphere (ICRU, 1980) was used to calculate the dose to tissue from neutrons traveling through a given distance of tissue. The source material was placed in the center of the sphere and dose rate tallies were recorded at the surface of the RMFC, and through 1, 2, 5, 10, 15, 20 25, and 30 centimeters of ICRU defined tissue equivalent material. The distance between different organs in the body is tabulated in Table 3.4. This table can be used in conjunction with results presented in Section 4.3 to determine the dose to various organs, depending on the location of the RMFC.

[11] Project goals required that the RMFC be contained in a volume of 1-2 cm^3 (DARPA).

Table 3.5 Distance (cm) from center-points of selected organs for use with ICRU sphere

	Adrenal	Bladder	Stomach	Small Int.	Ascending U.L.I.	Transverse U.L.I	Descending Colon	Transverse Colon	Heart
Adrenal	—	32.3	11.5	19.6	25.0	17.2	22.7	33.4	17.0
Bladder	32.3	—	28.2	14.0	14.5	17.5	14.3	1.3	43.0
Stomach	11.5	28.2	—	15.3	22.5	12.4	16.4	29.4	18.4
Small Int.	19.6	14.0	15.3	—	8.8	3.6	10.1	15.3	29.0
Ascending U.L.I.	25.0	14.5	22.5	8.8	—	10.3	18.0	15.5	32.2
Transverse U.L.I	17.2	17.5	12.4	3.6	10.3	—	11.7	18.8	25.6
Descending Colon	22.7	14.3	16.4	10.1	18.0	11.7	—	15.3	34.0
Transverse Colon	33.4	1.3	29.4	15.3	15.5	18.8	15.3	—	44.3
Heart	17.0	43.0	18.4	29.0	32.2	25.6	34.0	44.3	—
Kidney	5.7	27.3	10.5	15.6	22.0	14.0	17.6	28.4	21.7
Liver	8.5	27.4	8.9	13.5	18.1	10.5	19.4	28.6	16.3
Left Lung	18.6	48.0	20.4	34.3	39.4	31.0	36.6	49.2	10.7
Left Ovary	23.9	10.3	20.5	10.0	15.9	12.9	6.7	11.1	36.8
Pancreas	8.0	29.3	9.2	15.5	19.8	12.3	21.1	30.6	14.4
Spleen	7.4	31.9	7.9	19.8	27.1	17.6	19.8	33.1	19.4
Left Testicle	41.4	10.6	37.9	24.4	24.2	27.9	22.6	9.3	53.4
Thyroid	37.0	64.5	38.4	50.5	53.5	47.0	54.7	65.8	21.7
Uterus	31.0	2.5	26.3	12.2	13.0	15.6	13.0	3.7	41.1

Table 3.5 Distance (cm) from center-points of selected organs for use with ICRU sphere

	Kidney	Liver	Left Lung	Left Ovary	Pancreas	Spleen	Left Testicle	Thyroid	Uterus
Adrenal	5.7	8.5	18.6	23.9	8.0	7.4	41.4	37.0	31.0
Bladder	27.3	27.4	48.0	10.3	29.3	31.9	10.6	64.5	2.5
Stomach	10.5	8.9	20.4	20.5	9.2	7.9	37.9	38.4	26.3
Small Int.	15.6	13.5	34.3	10.0	15.5	19.8	24.4	50.5	12.2
Ascending U.L.I.	22.0	18.1	39.4	15.9	19.8	27.1	24.2	53.5	13.0
Transverse U.L.I.	14.0	10.5	31.0	12.9	12.3	17.6	27.9	47.0	15.6
Descending Colon	17.6	19.4	36.6	6.7	21.1	38.7	3.4	72.7	13.0
Transverse Colon	28.4	28.6	49.2	11.1	30.6	33.1	9.3	65.8	3.7
Heart	21.7	16.3	10.7	36.8	14.4	19.4	53.4	21.7	41.1
Kidney	—	8.8	23.4	18.5	9.6	7.4	36.1	42.2	26.2
Liver	8.8	—	21.7	20.9	2.0	11.6	37.4	38.0	25.7
Left Lung	23.4	21.7	—	40.1	19.9	18.4	57.8	20.4	46.2
Left Ovary	18.5	20.9	40.1	—	22.8	22.8	18.1	58.1	9.8
Pancreas	9.6	2.0	19.9	22.8	—	11.4	39.4	36.0	27.7
Spleen	7.4	11.6	18.4	22.8	11.4	—	40.8	38.2	30.5
Left Testicle	36.1	37.4	57.8	18.1	39.4	40.8	—	74.9	12.9
Thyroid	42.2	38.0	20.4	58.1	36.0	38.2	74.9	—	62.5
Uterus	26.2	25.7	46.2	9.8	27.7	30.5	12.9	62.5	—

(continued)

3.6 Plutonium Dispersion Modeling with HOTSPOT

, The computer code HOTSPOT (Homann, 2005) can be used to model the consequences of a release of PuO_2 to the environment following a breach of the structural integrity of the RMFC. HOTSPOT can model the area of the plume for various environmental conditions and estimate the resultant dose to individuals in the plume's path. HOTSPOT is distributed by Lawrence Livermore National Laboratory. The code uses a Gaussian plume model shown in Equation 3.6 to perform safety analysis in the event of an airborne release of a single radionuclide, or mixture of up to fifty radionuclides:

$$X(x,y,z) = \frac{Q}{2\pi\sigma_y\sigma_z u} \cdot e^{-\frac{1}{2}\left(\frac{y}{\sigma_y}\right)^2} e^{-\frac{1}{2}\left(\frac{z-h_e}{\sigma_z}\right)^2} e^{-\frac{1}{2}\left(\frac{z+h_e}{\sigma_z}\right)^2} \quad \textbf{(3.6)}$$

where X = concentration (Ci/m^3) at a point (x,y,z); Q = source strength; σ_z σ_y = crosswind and vertical plume standard deviation of plume concentration; u = mean wind speed, and h_e = height of the release point.

The three-dimensional modeling capabilities of the code can be used to simulate a release via explosion, fire, resuspension (from a surface deposit), or continuous release plume modeling. The HOTSPOT computer code was used to analyze a hypothesized release of source material from the RMFC and the immediate dispersal of material into the atmosphere using the explosion scenario model.

It was assumed that all 17 Ci of ^{238}Pu were available for dispersion after the explosive event occurs. The parameters of the release scenario are intended to simulate a RMFC that has been compromised and all of the source material is released

to the atmosphere. In addition to 100% of the material being released to the atmosphere, 100% of the material was also considered to be respirable (diameter of particles < 10 μm). This is a reasonable assumption because particles with diameters above 10 μm experience greater than 25% self absorption of α's (Misner, 2005) which is not desirable for efficient radiolytic hydrogen production.

In order to cover the gamut of exposure scenarios, deposition velocities (V_d) of 0.0, 0.1 cm/s (Whicker and Schultz, 1982), and 0.3 cm/s (Healy, 1974) were selected for the radionuclide. The scenarios also considered variable wind speeds of 0.1, 2.0, 5.0, and 10.0 m/s, and explosive forces of 0.0, 1, 10, and 100 equivalent lbs of TNT. Atmospheric stability classes[12] F (most stable) and A (least stable) were analyzed for each proposed exposure scenario as well. The HOTSPOT output values are summarized in Chapter 4.

HOTSPOT is capable of producing three simultaneous dose contours. The three dose contours selected were the acute (1-day) 10 Gy and 5 Gy adjusted dose to the lungs (NUREG/CR-4214, 1993) and the 0.5 Sv committed dose equivalent to the bone surface. HOTSPOT was also used to determine the ground deposition (kBq/m^2) for input into the RESRAD environmental radionuclide transport code.

[12] Stability classes correspond to σ_y, $\sigma_z = \sigma_\theta$ Class F, $\sigma_\theta = 2.5°$; Class E, $\sigma_\theta = 5°$; Class D, $\sigma_\theta = 10°$; Class C, $\sigma_\theta = 15°$; Class B, $\sigma_\theta = 20°$; Class A, $\sigma_\theta = 25°$.

3.7 Utilization of RESRAD for Environmental Transport of Plutonium

To assess the consequences of deposition of PuO_2 to the ground and resultant exposure pathways up to 1000 years after the initial event, the computer code RESRAD was used. The RESRAD computer code was developed in the Environmental Assessment Division at Argonne National Laboratory (EADANL, 2005). RESRAD can be used to calculate doses to individuals from surface deposition of radionuclides. This is particularly useful because dose to humans due to residual radioactivity at a point in time depends on a variety of parameters: initial deposition,radioactive decay, modes of transport, and removal and uptake, through both environmental and biological compartments. RESRAD allows the user to modify and examine the factors that affect the ultimate rate of transport, and removal (and non-removal) of nuclides from a system. Thus, the cumulative dose received by a hypothetical individual and the exposure pathways which contributed to the resultant dose can be examined.

The Nuclear Regulatory Commission has approved and uses the RESRAD family of codes to evaluate dose and residual activity limits at sites that are undergoing remediation or being decommissioned.

The Savannah River Site (SRS) near Aiken, South Carolina, has been selected as a test (simulation) location to employ RESRAD for the calculation of PuO_2 deposition from a failed RMFC. The SRS was selected because there is a substantial amount of literature about the site, which negates the need for independent soil analysis and measurement of environmental parameters.

RESRAD contains a set of default parameters, which can be modified by the user to simulate a specific site. Table 3.7 shows the input parameters used to model the area surrounding the Savannah River Site.

Table 3.7 RESRAD parameters modified from their default values.

Parameter	Value	Units	Default value	Reference
Transport Factor	5	cm^3/g	2000	USEPARSP
Solubility Limit	1E-08	[M] mol/L	0	Fujiwara, 2002
Contaminated Zone				
Area	570,000	M^2	10000	HOTSPOT output
Thickness	0.001	M	2.0	Scenario Specific
Soil Density	1.65	$g \cdot cm^{-3}$	1.5	Simpkins, 2001
Cover				
Erosion rate	0.001	$m \cdot yr^{-1}$	0.001	Simpkins, 2001
Wind speed	3.83	$m \cdot s^{-1}$	2.0	Jannik, G.T.
Precipitation	1.3	$m \cdot yr^{-1}$	1	Jannik, G.T.
Total Soil Porosity	0.359	%	0.4	Simpkins, 2001
Hydraulic Conductivity	11.2	$m \cdot yr^{-1}$	10	Simpkins, 2001
Occupancy				
Mass Loading	0.001	$m \cdot yr^{-1}$	0.0001	Simpkins, 2001
% Time Spent Outdoors	100%	%	40%	Assumed
Ingestion Pathways				
Drinking Water Intake	600	$Liters \cdot yr^{-1}$	510	Hunter, 2004

Explanation of Parameters

The following site-specific and default exposure parameters were used as input values for the RESRAD calculations. All of the parameters modified from their default values are summarized in Table 3.7.

a) Transport Factor

The transport factor was set at 5 cm^3/g (USEPARSP, 2005). This value is from a protocol for plutonium published by the EPA. The default value is 2000 cm^3/g. The smaller value means that the contaminant is transferred away from the site faster than the default value. Defined as the ratio of contaminant (PuO_2 in this case) in the solid phase to the concentration in surrounding aqueous solution.

b) Area of Contaminated Zone

An area of 570,000 m^2 was used for the area of the contaminated zone. This area is assumed to be circular.

c) Thickness of Contaminated Zone

A radiological contaminated zone thickness of 0.001m was used for the volume contamination calculations. The soil at SRS is a clay loam that readily holds the contaminants on the surface. This also kept the thickness of the contaminated zone following initial deposition to a minimum.

d) Cover Depth

The cover depth used was 0 m, indicating no shielding by uncontaminated soil.

e) Density of Contaminated Zone

The contaminated zone density was assumed to be 1.65g/cm^3, which was a parameter used for another study of SRS soil type (Simpkins, 2001).

f) Contaminated Zone Erosion Rate

For the contaminated soil, the contaminated zone erosion rate used was 0.001 m/y. This is the default erosion rate used in RESRAD and supported is supported by Simpkins 2001 study (Simpkins, 2001).

g) Contaminated Zone Total Porosity

The contaminated zone total porosity used was .359. This was determined using data from SRS soil contamination study (Simpkins, 2001).

h) *Contaminated Zone Hydraulic Conductivity*

To account for the contaminated soil, the contaminated zone hydraulic conductively was assumed to be 11.2 m/y (Simpkins, 2001).

i) Average Annual Wind Speed

The SRS site-specific value of 3.83 m/s, measured during the years 1997 to 2001, was used for the average annual wind speed parameter (Jannik, G.T.).

j) Evapotranspiration Coefficient

The RESRAD default value of 0.5 was used for the evapotranspiration coefficient. Defined as the ratio of water in the root zone transferred to the atmosphere.

k) Precipitation Rate

The SRS site-specific value of 1.3 m/yr was used for the precipitation rate parameter (Jannik, G.T.).

l) Irrigation Rate

The default irrigation rate parameter used was 0.2 m/yr was used.

m) Inhalation Rate

The annualized inhalation rate used for the industrial worker was 8400 m^3/y. This rate is the RESRAD default value.

n) Mass Loading for Inhalation

A value of 0.001 g/m^3 was used for mass loading. This value is larger than the default by an order of magnitude. This is because the deposition event occurs on the surface. Using this value should keep our inhalation dose estimate conservative.

o) Exposure Duration

The exposure duration used was 30 y, the default public duration.

p) Fraction of Time Spent Indoors

The fraction of time spent indoors onsite individual was conservatively set at 0.0, indicating that the people around the contamination would spend none of their time indoors shielded by buildings.

q) Fraction of Time Spent Outdoors

The fraction of time spent outdoors was set at of 1.0.

r) Soil Ingestion Rate

The annualized soil ingestion rate used for the onsite individual was 36.5 g/year. This is the rate specified by the EPA.

s) Drinking water intake

Drinking water intake was set at 600 liter/year to account for the warm temperatures in South Carolina (Hunter, 2004).

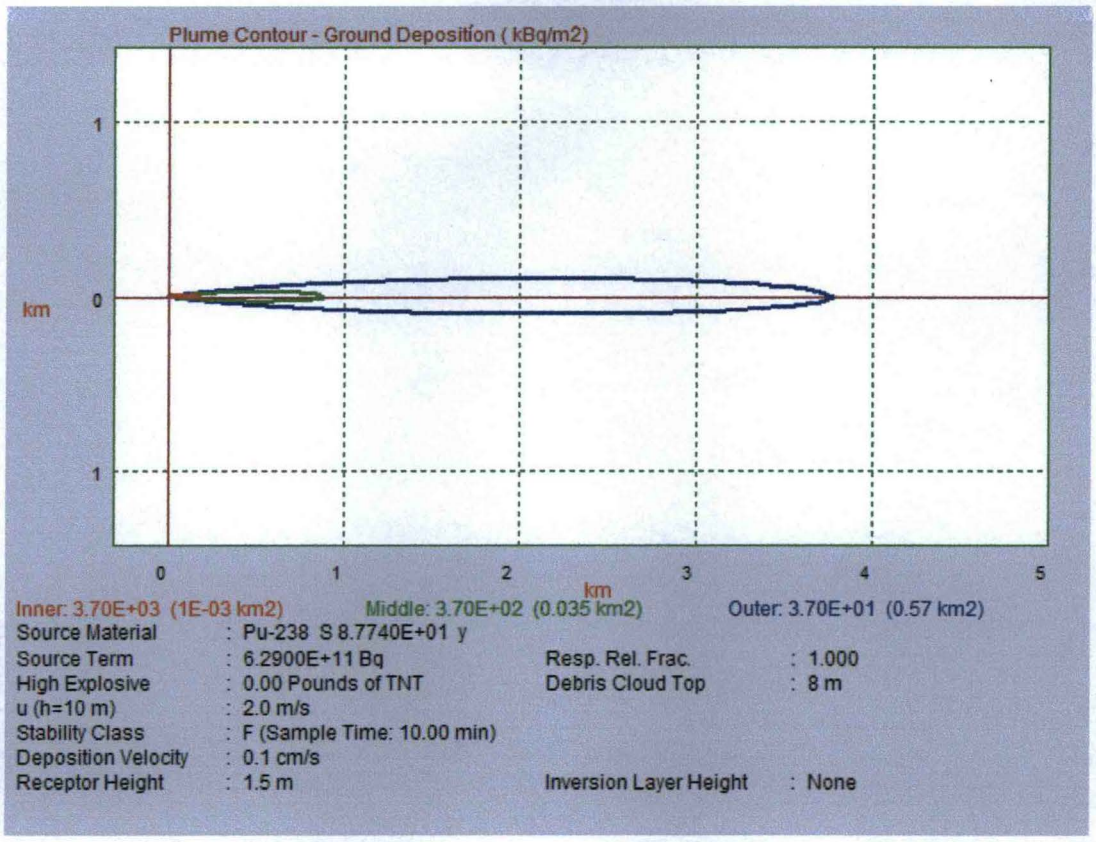

Figure 3.7 HOTSPOT deposition contour plot used to determine RESRAD contaminated area

Figure 3.7 shows the HOTSPOT deposition contour plot used to determine the activity concentration of plutonium and contaminated area for input into RESRAD. These conditions were selected because the dose contour plot area was largest for the physical parameters listed above in Figure 3.7. The weighted average concentration for the contaminated area was calculated from the HOTSPOT deposition contour plot shown in Figure 3.7. The thickness of the contaminated soil was assumed to be 0.001 m and the density of the soil to be 1.65 g/cm^3. The activity concentration was calculated to be 0.038 kBq/g of soil and the calculation is shown in Equation 3.7.

This scenario was chosen to be the bounding case contamination area because of the large area of the contaminated zone. All other combinations of stability classes and wind speeds would yield a smaller contamination area.

$$\left(\frac{\left[\frac{(3700\,kBq \cdot 1E03) + (370\,kBq \cdot 3.5E04) + (37\,kBq \cdot 5.35E05)}{5.7E05\,m^2} \right]}{\frac{0.001\,m\,(\text{thickness of contaminated zone})}{1.65E06\,g/m^3\,(\text{soil density})}} \right) = 0.038\,kBq/g \quad \textbf{(3.7)}$$

4. RESULTS & DISCUSSION

4.1 Neutron Source Strength

The neutron source strength was determined using the geometry described in Section 3.2 and using either mono-energetic or energy dependent (α,n) reaction cross sections for α-particles of energy 5.5 MeV. Additionally, the neutron source strength was calculated for two conditions: O(α,n)Ne reactions taking place in the oxide fuel or in the oxygen atoms in the H_2O. The results are illustrated in Table 4.1.

Table 4.1 Neutrons per second emitted from RMFC determined from energy deposited in PuO_2 or H_2O. Considered for mono-energetic and energy dependent (α,n) cross sections.

Reaction Cross Section $\sigma_{\alpha,n}$	α-Energy Deposition	Neutron Source (neutrons·s^{-1})
mono-energetic $\sigma_{\alpha,n}$(5.5MeV)	$^{238}PuO_2$	1.56E04
energy-dependent $\sigma_{\alpha,n}$(E)	$^{238}PuO_2$	1.21E04
$\sigma_{\alpha,n}$(5.5MeV)	H_2O	3.35E04
$\sigma_{\alpha,n}$(E)	H_2O	2.6E04

The magnitude of the dose to personnel is directly proportional to the source strength of particles emitted from the source. As can be seen in Table 4.l, employing the energy dependent (α,n) reaction cross sections to calculate the reaction rate reduces the neutron source strength by 22% from the mono-energetic reaction cross section at 5.5 MeV. The calculation using the energy spectrum is the more accurate

result. MCNPX can determine the energy of the alpha particle causing the collision and assign the corresponding reaction cross section to calculate the interaction rate.

The literature reviewed in Chapter 2 (Anderson, 1980 & 1985) provides neutron spectral information and neutrons produced per second per gram of material. The results in these papers are within 30% percent of neutron source strength determined using MCNPX. However, both of the experiments conducted were characterizing the neutron strength resulting from interactions in the PuO_2. For the RMFC to operate (and generate hydrogen), the α-particles need to deposit their energy in the water. This second situation was modeled as well, and it produced a neutron source strength over a factor of two higher than (α,n) reactions occurring in the PuO_2. Again, this seems to be a more accurate representation of the physical situation that we wish to model. The neutron source strength used for dosimetry calculations in the sections that follow consider (O(α,n)Ne) neutrons produced in PuO_2 and H_2O using the energy dependent reaction cross sections.

4.2 Neutron Dose to Personnel @ 30 cm

Specific RMFC project goals require the calculation of dose rate to personnel 30 cm from the fuel cell (DARPA,2004). The neutron source strength was determined with different physical and geometrical considerations taken into account, with the four most prudent scenarios presented previously in Table 4.1. The neutron dose depends not only on the number of neutrons emitted from the source per second, but also on the energy spectra of the source neutrons. Table 4.2a and 4.2b show the

calculated dose at 30 cm from the simulated RMFC from neutrons produced in the plutonium oxide and in water using several neutron energy spectra.

Table 4.2a Neutron dose rate resulting from O(α,n)Ne reactions occurring in PuO_2. Considered for a mono-energetic source and three published neutron energy spectra.

Neutron Source neutrons·s^{-1}	**Energy Spectrum**	**MCNP output** Rem/hr	**mrem/yr** @ 30 cm
1.21E04	-mono- 5.5MeV	1.42E-04	1240
1.21E04	1.19g $^{238}PuO_2$ (Anderson, 1980)	1.23E-04	1070
1.21E04	10kg PuO_2 (Anderson, 1985)	1.05E-04	920
1.21E04	Mixed oxide fuel (Babut, 2004)	1.09E-04	960

Table 4.2b Neutron dose rate resulting from O(α,n)Ne reactions occurring in H_2O. Considered for a mono-energetic source and three published neutron energy spectra.

Neutron Source neutrons·s^{-1}	**Energy Spectrum**	**MCNP output** Rem/hr	**mrem/yr** @ 30 cm
2.6E04	-mono- 5.5MeV	2.95E-04	2580
2.6E04	1.19g $^{238}PuO_2$ (Anderson, 1980)	2.54E-04	2220
2.6E04	10kg PuO_2 (Anderson, 1985)	2.17E-04	1900
2.6E04	Mixed oxide fuel (Babut, 2004)	2.24E-04	1970

The calculated neutron dose to personnel at a distance of 30 cm from the RMFC is greatest when it is assumed that all the neutrons emitted from the source occur at 5.5 MeV and the neutron source is derived from (α,n) reactions in H_2O rather than PuO_2. Tables 4.2a and 4.2b illustrate how the dose is affected by differing the

assumed energy spectrum of neutrons emitted from the source. The mono-energetic neutron source results in the highest dose to personnel 30 cm from the RMFC. The energy spectrum which produces the second highest dose (Anderson, 1980) is used for the remainder of this analysis. It is felt that this spectrum is a reasonable choice for two reasons: the value of the dose calculated with this spectrum is just above the average of the doses computed under the four different considerations for neutron spectral information, and the 1.19 g PuO_2 source in this paper most closely resembles the physical characteristics of the PuO_2 that will be employed for use with the RMFC. The dose rate of 2220 mrem/yr is assumed for constant exposure at a distance 30 cm from the device. A standard 2000 hour working year yields a dose of 500 mrem/yr. The hourly dose rate of 0.25 mrem/hr is nearly the same as the dose rate onboard a commercial airplane (CACAQ, 1986).

4.3 Modified MIRD Phantom Results

Table 4.3a Annual dose to organs resulting from RMFC placed in pacemaker orientation

Placement	Pacemaker (rem/hr)	1 year (mrem/yr)	Tissue Weighting Factor	Effective Dose (mrem/yr)
Stomach	2.60E-05	2.28E+02	0.12	2.74E+01
Small Intestine	8.07E-07	7.07E+00	*	2.83E+00
Large Intestine	1.40E-06	1.23E+01	*	7.69E-02
Descending Colon	3.50E-07	3.07E+00	0.12	3.68E-01
Transverse Colon	1.20E-07	1.05E+00	0.12	1.26E-01
Heart	5.40E-04	4.73E+03	*	2.96E+01
Kidney	6.80E-06	5.96E+01	*	3.73E-01
Liver	1.45E-05	1.27E+02	0.05	7.94E-01
Lung	1.86E-03	1.63E+04	0.12	1.96E+03
Ovary	1.10E-07	9.64E-01	0.20	1.93E-01
Pancreas	1.25E-05	1.10E+02	*	6.88E-01
Spleen	2.50E-05	2.19E+02	*	1.37E+00
Testicle	0.00E+00	0.00E+00	0.20	0.00E+00
Thymus	1.33E-03	1.17E+04	*	7.31E+01
Thyroid	9.80E-05	8.58E+02	0.05	5.36E+00
Uterus	2.80E-08	2.45E-01	*	1.53E-03
Adrenal	2.60E-05	2.28E+02	*	1.43E+00
Bladder	7.00E-09	6.13E-02	0.05	3.83E-04
Total Effective Dose (mrem/yr)				2.104E+03

* the weighting factor 0.05 is applied to the average dose of these organs

Table 4.3b Dose to individual organs and total effective dose equivalent resulting from 'digestion' of RMFC

Placement	Stomach (rem/hr) Residence time = 1 hr	Stomach (mrem) 1hr	Small Intestine (rem/hr) Residence time = 4 hr	Small Intestine (mrem 4 hr)	Large Intestine (rem/hr) Residence time = 13 h	Large Intestine (mrem 13 hr)	Colon (rem/hr) Residence time = 24 hr	Colon (mrem 24 hr)	Tissue Weighting Factor	Effective Dose (mrem)
Stomach	1 20E-02	1 20E+01	3 90E-04	1 56E+00	3 40E-02	1 02E+02	3 30E-05	7 92E-01	0 12	1 40E+01
Small Intestine	3 20E-04	3 20E-01	7 90E-03	3 16E+01	3 20E-04	9 60E-01	9 70E-04	2 33E+01	*	3 51E-01
Large Intestine	7 70E-04	7 70E-01	5 70E-03	2 28E+01	7 60E-04	2 28E+00	8 40E-04	2 02E+01	*	2 88E-01
Descend	2 80E-04	2 80E-01	1 20E-03	4 80E+00	2 80E-04	8 40E-01	7 80E-04	1 87E+01	0 12	2 95E+00
Transverse Colon	3 40E-05	3 40E-02	1 20E-03	4 80E+00	3 40E-05	1 02E-01	4 20E-02	1 01E+03	0 12	1 22E+02
Heart	1 40E-04	1 40E-01	1 10E-05	4 40E-02	1 40E-04	4 20E-01	7 90E-07	1 90E-02	*	3 89E-03
Kidney	1 10E-03	1 10E+00	3 90E-04	1 56E+00	1 10E-03	3 30E+00	3 00E-05	7 20E-01	*	4 18E-02
Liver	2 80E-04	2 80E-01	1 80E-04	7 20E-01	2 80E-04	8 40E-01	1 70E-05	4 08E-01	0 05	1 41E-02
Lung	3 10E-04	3 10E-01	9 10E-06	3 64E-02	3 10E-04	9 30E-01	7 70E-07	1 85E-02	0 12	1 55E-01
Ovary	7 60E-05	7 60E-02	1 70E-03	6 80E+00	7 10E-05	2 13E-01	2 40E-03	5 76E+01	0 20	1 29E+01
Pancreas	1 40E-03	1 40E+00	1 50E-04	6 00E-01	1 40E-03	4 20E+00	9 50E-06	2 28E-01	*	4 02E-02
Spleen	2 60E-03	2 60E+00	1 20E-04	4 80E-01	2 60E-03	7 80E+00	1 10E-05	2 64E-01	*	6 97E-02
Testicle	0 00E+00	0 00E+00	0 00E+00	0 00E+00	0 00E+00	0 00E+00	0 00E+00	0 00E+00	0 20	0 00E+00
Thymus	1 40E-05	1 40E-02	1 20E-06	4 80E-03	1 30E-05	3 90E-02	5 70E-08	1 37E-03	*	3 70E-04
Thyroid	1 10E-07	1 10E-04	7 20E-10	2 88E-06	4 80E-07	1 44E-03	0 00E+00	0 00E+00	0 05	9 71E-06
Uterus	1 60E-05	1 60E-02	6 70E-04	2 68E+00	1 60E-05	4 80E-02	8 40E-03	2 02E+02	*	1 28E+00
Adrenal	7 20E-04	7 20E-01	8 10E-05	3 24E-01	7 20E-04	2 16E+00	5 90E-06	1 42E-01	*	2 09E-02
Bladder	5 20E-06	5 20E-03	1 70E-04	6 80E-01	5 16E-06	1 55E-02	4 60E-03	1 10E+02	0 05	6 92E-01
								Total Effective Dose Equivalent (mrem)		1 519E+02

* The weighting factor 0.05 is applied to the average dose for these organs

The resulting doses to the organs modeled in the modified MIRD phantom are presented in Tables 4.3a and 4.3b. Table 4.3a shows the doses to individual organs over a one year time period as result of placing an RMFC inside the chest cavity in the typical location of a pacemaker (Arnold, 1973). The left lung is subjected to the highest dose rate: 16.3 rem/yr. The heart receives an equivalent dose in one year of 4.73 rem.

NUREG/CR-4214 (1993) guidelines suggest that an acute dose of 5 Gy equivalent, in one day, is the threshold dose for which deterministic irritation of the pulmonary region of the respiratory tract begins to occur. Deterministic complications to cardiac tissue occur at doses of 4,000 rads received in a one month time period (Arnold, 1973). Above this rate, tissue lesions have been documented and cardiac tissue has been observed to experience inflammation, leaking of intracellular fluid, and loss of elasticity by way of increased fibrous tissue (Arnold, 1973). As a result, no adverse acute effects would result from implantation of such a device in the chest cavity.

The total effective dose equivalent (TEDE) in one year resulting from implantation of an RMFC is 2.1 rem. Because the modified MIRD phantom does not include the red marrow, breast, or esophagus, the TEDE could be as high as 5.7 rem/yr. This is calculated using the conservative assumption that the red marrow, breast, and esophagus all receive an equivalent dose equal to that of the left lung, which was the organ that received the highest dose in this portion of the analysis.

Using EPA's risk factor[13] (USEPA, 2006) the relative risk of developing a fatal cancer is 0.36%.

The dose tallies for the organs modeled in the MIRD phantom for this portion of the analysis have relative error (RE) of less than 5%. The exceptions are the colon (25% RE), ovary (54% RE), uterus (40% RE), and bladder (37% RE). As can be seen in Table 4.4a, the organs with large associated errors contributed less than 5 mrem/yr. Using the largest relative error of any organ (the ovary),there is still 95% confidence that the cumulative dose to these four organs is less than10 mrem/yr.

The modified MIRD phantom was also used to calculate the dose to the gastrointestinal tract and other organ to determine if any acute radiation effects would result from ingestion of an intact RMFC, and to calculate the TEDE in order to quantify the relative risk associated with ingestion of the micro-fuel cell. Table 4.3c shows NUREG/CR-4214 (1993) values of thresholds and LD_{50}[14] dose for the red marrow, small intestine, lung, ovary, and testes.

Table 4.3c Threshold and LD_{50} values for deterministic effects to the small intestine, lung, red marrow, and gonads resulting from acute doses

	Threshold (rad)	$LD_{50/60}$ (rad)
Red Marrow	150	300
Small Intestine	750	1500
Lung	500	1000
Ovary	60	350
Testes	30	70

(NUREG/CR-4214, 1993)

[13] The relative risk of developing a fatal cancer is $(5<6)x10^{-4}$/rem (USEPA, 2006).
[14] Dose of radiation required to kill, within a specified period, 50 percent of the individuals in the population. $LD_{50/T}$, where T for human populations is usually set at 30 or 60 days.

The thresholds shown in Table 4.3c are not approached in the simulated results. Although the values given in Table 4.3c are in absorbed dose (rad) and the values in Table 4.3b are given in equivalent dose (mrem) the values are comparable and the equivalent dose is orders of magnitude below the threshold for deterministic effects given in the NUREG guidelines. Only stochastic relative cancer risk can be evaluated.

The TEDE calculated for digestion of the RMFC is 150 mrem. As with the pacemaker TEDE calculation, the phantom did not include red marrow, breasts, or an esophagus. The colon received the highest equivalent dose as a result of the fuel cell passing through the gastrointestinal tract. The equivalent dose received by the colon was 1 rem. If we assume the red marrow, breasts and esophagus all received 1 rem as well, the upper bound for the TEDE is 175 mrem. According to the linear no threshold risk/dose model, this radiation dose would equate to a relative increase in cancer risk of 1 in 10,000.

The dose tallies for the majority of organs modeled in the MIRD phantom for the digested RMFC analysis have less than 5% relative error. However, there are exceptions. While the RMFC is in the stomach, the thyroid dose tally has 45% relative error (RE). During digestion, while the RMFC resides in the small intestine, the small intestine, the thymus, and thyroid dose tallies have respective relative errors of 18% and 72%. The thyroid dose estimate has 32% associated relative error while the RMFC is in the large intestine. The kidney, thymus, and adrenal dose estimates have respective relative errors of 67%, 73%, and 10% when the RMFC resides in the

colon. The cumulative dose to the organs with large associated relative errors is less than 1 mrem. Larger relative errors in dose are observed for organs that are farther from the RMFC. These organs have a minimal impact on the cumulative dose. The organs with large relative errors do not have a significant effect on the accuracy of the calculated total effective dose equivalent.

4.4 Neutron Dose Through Tissue

The neutron dose through a given length or thickness of human tissue was evaluated using the ICRU reference sphere (ICRU, 1980). The dose to tissue at different distances from the neutron source is important when evaluating the dose to the body and organs from RMFC ingestion or implantation. The dose rates calculated by MCNP5 for varying depths of tissue are presented in Table 4.4a and 4.4b for neutrons generated in PuO_2 and H_2O, respectively.

Table 4.4a Dose rates to tissue at given distances from RMFC inside the body given neutron source from all (α,n) reactions occurring in PuO_2.

Dose rate @surface	@1cm	@2cm	@5cm	@10cm	@15cm	@20cm	@25cm	@30cm
mrem/hr								
300	69	21	3.1	0.48	0.11	0.032	0.01	0.003
mrem/yr								
2.7E06	6E05	1.8E05	2.7E04	4.2E03	1E03	2.78E02	8.4E01	2.8E01

Table 4.4b Dose rates to tissue at given distances from RMFC inside the body given neutron source from all (α,n) reactions occurring in H_2O.

Dose rate @surface	@1cm	@2cm	@5cm	@10cm	@15cm	@20cm	@25cm	@30cm
mrem/hr	mrem/hr	mrem/hr	Mrem/hr	mrem/hr	mrem/hr	mrem/hr	mrem/hr	mrem/hr
640	150	45	6.7	1.03	0.24	0.07	0.021	0.0064
mrem/yr	mrem/yr	mrem/yr	Mrem/yr	mrem/yr	mrem/yr	mrem/yr	mrem/yr	mrem/yr
5.8E06	1.3E06	3.9E05	5.8E04	9.0E03	2.1E03	5.97E02	1.80E02	6.02E01

Figure 4.4a is a graphical representation of the neutron dose through tissue as a function of tissue thickness (0.0 cm (dose at surface) to 30 cm). The dose through 30 cm of tissue is much less than the dose through 30 cm of air reported in section 4.2. Originally, the ICRU reference sphere and dose through different tissue thicknesses was to be used to calculate the dose to the human body via ingestion or implantation of an RMFC. The construction of the modified MIRD phantom provides a more accurate assessment of the specific cases considered in this analysis. The neutron dose through tissue evaluation can still be useful when evaluating more generic exposure scenarios, as long as one knows the distance between the target and source organs.

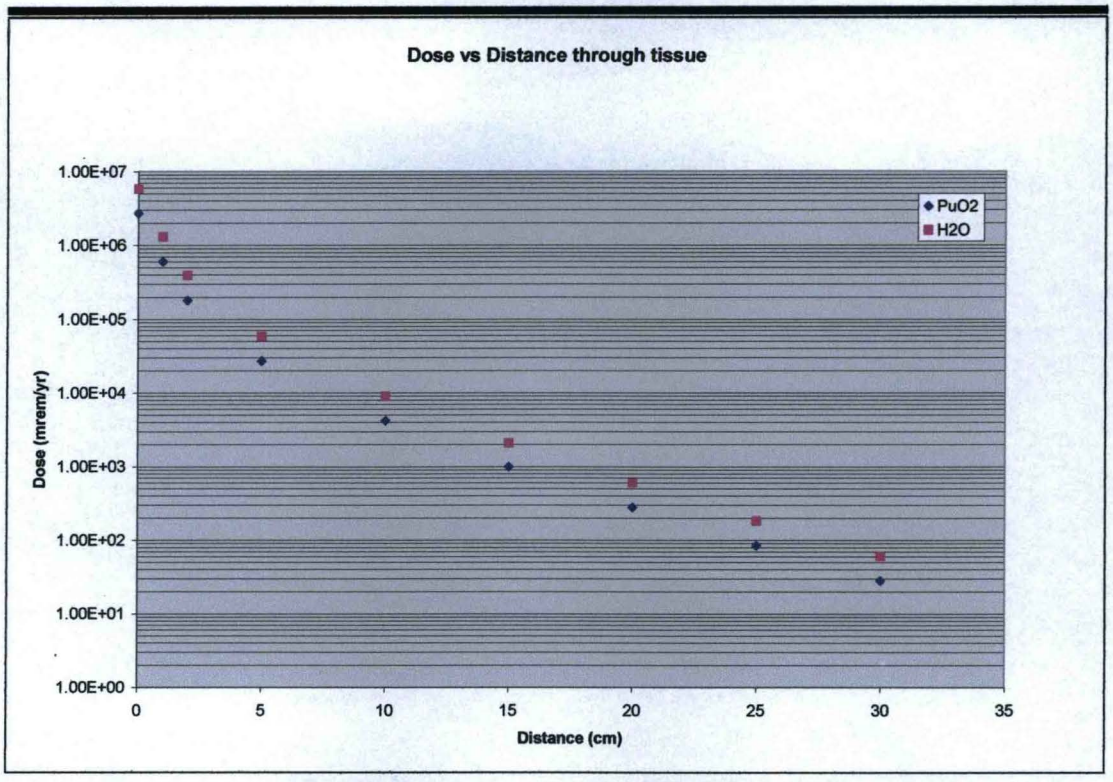

Figure 4.4a Dose to tissue as a function of distance from the RMFC neutron source inside the body, shown for neutrons produced in PuO_2 and H_2O.

Figure 4.4b compares the computed dose rates for an RMFC placed in the stomach using neutron dose through tissue results (Table 4.4b) and modified MIRD phantom results (Table 4.3b). The two methods yield comparable results. This table also shows that for other proposed internal dose scenarios the dose through tissue using the ICRU sphere is a useful tool.

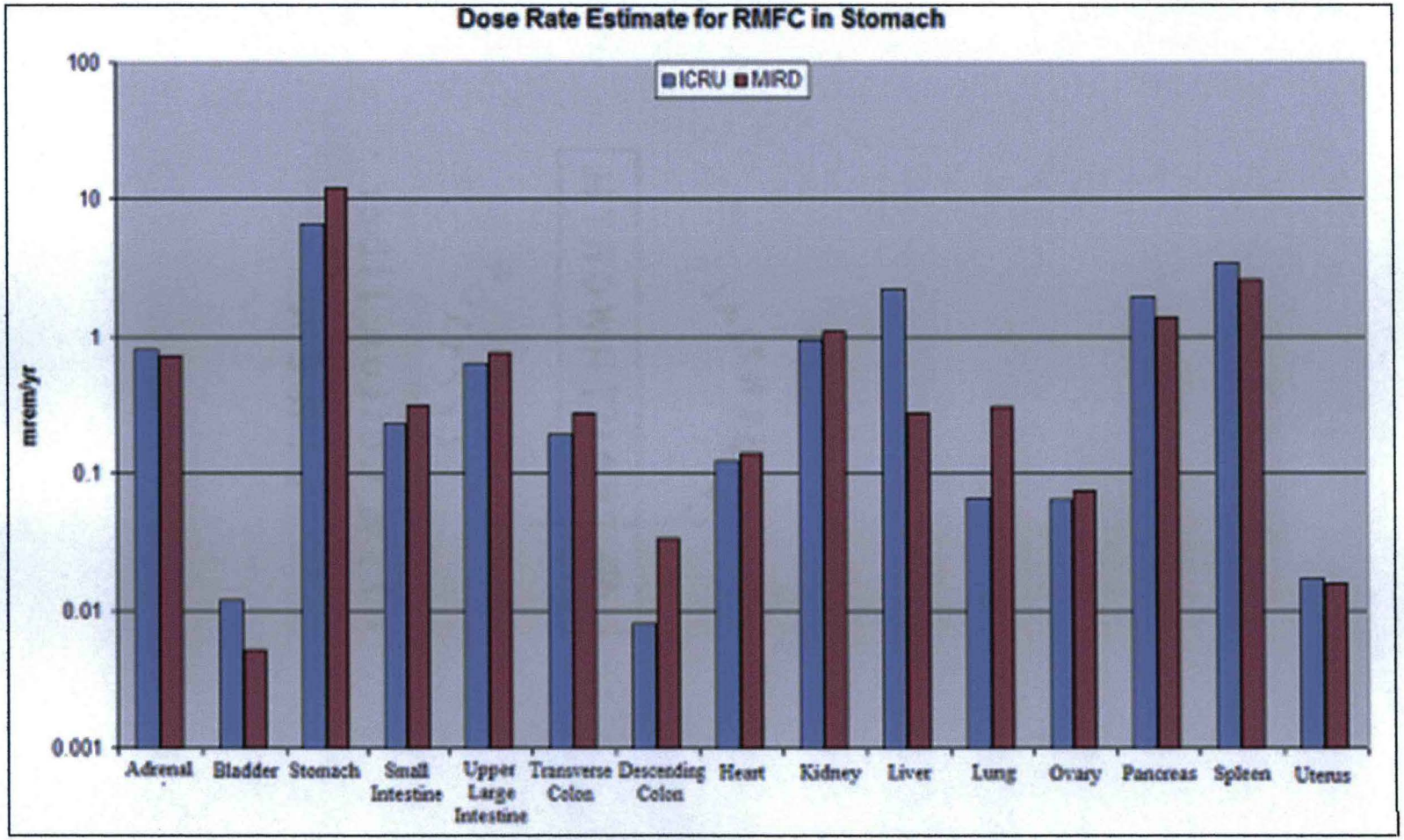

Figure 4.4b Comparison of MIRD phantom and ICRU sphere results for RMFC placed in the stomach

4.5 HOTSPOT Plutonium Dispersion

The results from the various scenarios analyzed with the HOTSPOT computer code are presented in Tables 4.5a through 4.5h. Each table contains the length of the plume centerline downwind from the PuO_2 release point and the area of the plume where the acute dose or committed dose equivalent would be received by an individual at the time the plume were to pass. An '—' in Tables 4.5a-g indicates the threshold was not surpassed for the conditions given.

Table 4.5a Effective length of plume centerline and effective area of plume downwind from release point, vs wind speed (V_d = 0.0 cm/s; stability class F).

V_d = 0.0 cm/s Stability Class F	Wind Speed 0.1 m/s	Wind Speed 2.0 m/s	Wind Speed 5.0 m/s	Wind Speed 10.0 m/s
LD_{50} 10 Gy*eq Lung	0.28 km (3E-03 km^2)	—	—	—
Threshold 5 Gy*eq Lung	0.45 km (0.60 km^2)	0.018 km (6E-03 km^2)	—	—
CDE 0.5 Sv Bone Surface	> 200 km	170 km (267 km^2)	0.68 km (0.13 km^2)	0.48 km (0.064 km^2)

Table 4.5b Effective length of plume centerline and effective area of plume downwind from release point, vs wind speed (V_d = 0.0 cm/s; stability class A).

V_d = 0.0 cm/s Stability Class A	Wind Speed 0.1 m/s	Wind Speed 2.0 m/s	Wind Speed 5.0 m/s	Wind Speed 10.0 m/s
LD_{50} 10 Gy*eq Lung	0.025 km (2E-04 km^2)	—	—	—
Threshold 5 Gy*eq Lung	0.04 km (9E-04 km^2)	—	—	—
CDE 0.5 Sv Bone Surface	5.3 km (6.7 km^2)	1.1 km (0.32 km^2)	0.68 km (0.13 km^2)	0.48 km (0.064 km^2)

Table 4.5c Effective length of plume centerline and effective area of plume downwind from release point, vs wind speed (V_d = 0.3 cm/s; stability class F).

V_d 0.3 cm/s Stability Class F	Wind Speed 0.1 m/s	Wind Speed 2.0 m/s	Wind Speed 5.0 m/s	Wind Speed 10.0 m/s
LD_{50} 10 Gy*eq Lung	0.1 km (7E-04 km^2)	—	—	—
Threshold 5 Gy*eq Lung	0.16 km (2E-03 km^2)	0.18 km (5E-04 km^2)	—	—
CDE 0.5 Sv Bone Surface	1.5 km (0.19 km^2)	14.5 km (7.8 km^2)	15.2 km (7.3 km^2)	11.5 km (4.0 km^2)

Table 4.5d Effective length of plume centerline and effective area of plume downwind from release point, vs wind speed (V_d = 0.3 cm/s; stability class A).

V_d = 0.3 cm/s Stability Class A	Wind Speed 0.1 m/s	Wind Speed 2.0 m/s	Wind Speed 5.0 m/s	Wind Speed 10.0 m/s
LD_{50} 10 Gy*eq Lung	0.025 km (2E-04 km^2)	—	—	—
Threshold 5 Gy*eq Lung	0.037 km (7E-04 km^2)	—	—	—
CDE 0.5 Sv Bone Surface	3.6 km (3.4 km^2)	1.1 km (0.31 km^2)	0.68 km (0.13 km^2)	0.048 km (0.064 km^2)

Table 4.5e Effective length of plume centerline and effective area of plume downwind from release point, vs wind speed (V_d = 0.1 cm/s; stability class F).

V_d = 0.1 cm/s Stability Class F	Wind Speed 0.1 m/s	Wind Speed 2.0 m/s	Wind Speed 5.0 m/s	Wind Speed 10.0 m/s
LD_{50} 10 Gy*eq Lung	0.16 km (1E-03 km^2)	—	—	—
Threshold 5 Gy*eq Lung	0.26 km (4E-03 km^2)	0.018 km (1E-03 km^2)	—	—
CDE 0.5 Sv Bone Surface	5.2 km (1.7 km^2)	34 km (30 km^2)	25 km (14 km^2)	13.5 km (5.2 km^2)

Table 4.5f Effective length of plume centerline and effective area of plume downwind from release point, vs wind speed (V_d = 0.1 cm/s; stability class A).

V_d = 0.1 cm/s Stability Class A	Wind Speed 0.1 m/s	Wind Speed 2.0 m/s	Wind Speed 5.0 m/s	Wind Speed 10.0 m/s
LD_{50} 10 Gy*eq Lung	0.025 km (2E-04 km^2)	—	—	—
Threshold 5 Gy*eq Lung	0.04 km (8E-04 km^2)	—	—	—
CDE 0.5 Sv Bone Surface	4.7 km (5.3 km^2)	1.1 km (0.32 km^2)	0.69 km (0.13 km^2)	0.048 km (0.062 km^2)

Table 4.5g Effective length of plume centerline and effective area of plume downwind from release point, vs pounds TNT vs wind speed (V_d = 0.1 cm/s; stability class F).

V_d = 0.1 cm/s Stability Class F Wind 0.1 m/s	0 lbs TNT	1 lbs TNT	10 lbs TNT	100 lbs TNT
LD_{50} 10 Gy*eq Lung	0.16 km (1E-03 km^2)	—	—	—
Threshold 5 Gy*eq Lung	0.26 km (4E-03 km^2)	—	—	—
CDE 0.5 Sv Bone Surface	0.025 km (2E-04 km^2)	12 km (7 km^2)	13 km (7.1 km^2)	10.5 km (4.7 km^2)

Table 4.5h Effective length of plume centerline and effective area of plume downwind from release point vs pounds TNT, vs wind speed (V_d = 0.1 cm/s; stability class A).

V_d = 0.1 cm/s Stability Class A Wind 0.1 m/s	≈ 0 lbs TNT	1 lbs TNT	10 lbs TNT	100 lbs TNT
LD_{50} 10 Gy*eq Lung	0.025 km (2E-04 km^2)	—	—	—
Threshold 5 Gy*eq Lung	0.04 km (8E-04 km^2)	—	—	—
CDE 0.5 Sv Bone Surface	4.7 km (5.3 km^2)	4.5 km (4.9 km^2)	4.4 km (4.8 km^2)	4.25 km (4.6 km^2)

The results from the dispersal scenarios obtained with HOTSPOT indicate there is a chance of lethality to individuals who may be in close proximity if the RMFC is compromised and the PuO_2 source material is released to the atmosphere. The most severe case is a zone downwind from the dispersal at a plume centerline distance of 280 m and total area of 3000 m^2. This scenario is somewhat unrealistic, however, because the deposition velocity of the airborne particle was set to 0.0 cm/s. The only factor influencing plume dilution was dispersion – particle settling was not modeled.

The only wind speed at which a lethal dose was observed was 0.1 m/s. For values of 2 m/s and greater, the plume is moving fast enough that individuals in the path of the plume centerline would not have a substantial opportunity to breathe in enough air with high enough concentration to receive a lethal dose. If the PuO_2 is dispersed with any amount of force (TNT), there are no appreciable deterministic effects.

The NUREG/CR-4214 (1993) dose conversion factor for acute one-day exposure due to inhalation of ^{238}Pu to the lung is 6.89E-07 Gy-equivalent per Becquerel. One would need to inhale 1.45E07 Bq to receive the $LD_{50/60}$ dose of 10 Gy-equivalent to the lung (NUREG/CR-4214, 1993). The Gy-equivalent is a measure of acute exposure to determine deterministic threshold effects. The Gy-equivalent is determined for high-LET radiations to be the product of the absorbed dose and relative biological effectiveness factor for acute effects. This should not be confused with the radiation weighting factor which is multiplied by the absorbed dose (Gy or rad) to obtain the dose equivalent (Sv or rem). The RBE for α-particles in this assessment has been set to 10, as per NUREG/CR-4214 (1993) guidelines, and is correlated to the ability of the radiation to produce acute deterministic effects (NUREG/CR-4214, 1993). The radiation weighting factor, W_R, for α-radiation is 20 and is used to calculate the probability of radiation to produce stochastic effects such as cancer.

4.6 RESRAD—Plutonium in the environment

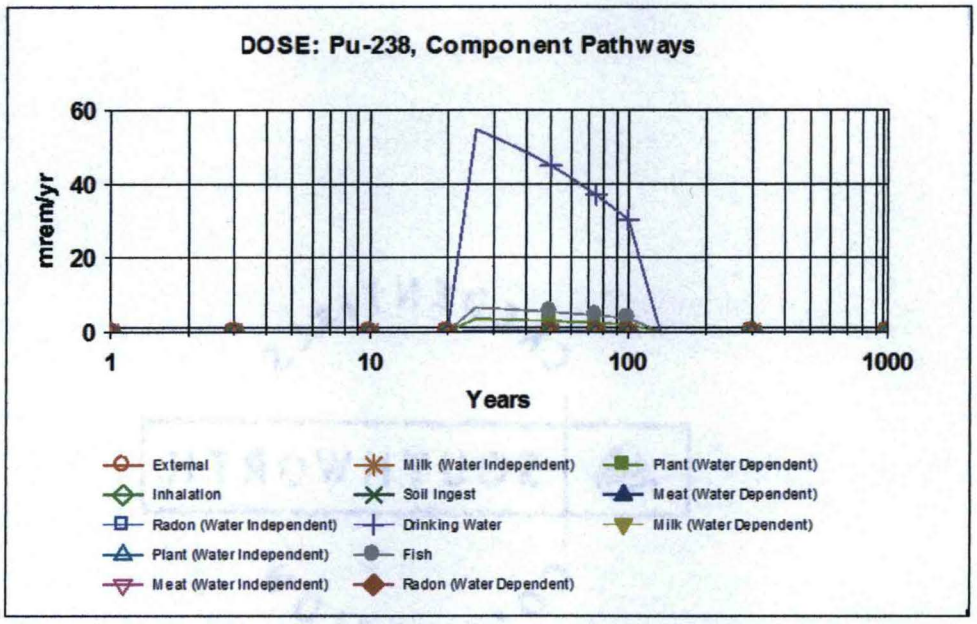

Figure 4.6a Dose to individuals living in the deposition zone shown by pathway in which dose is received vs. time in years.

The RESRAD output illustrated in Figure 4.6a indicates that the maximum dose to a hypothetical individual occurs 26 years after the initial deposition event. Individuals receive a radiation dose immediately after the initial deposition event because of inhalation of resuspended particles. One year later it is assumed that all the plutonium has migrated below the surface and is no longer available to be resuspended in the atmosphere. Based on the parameters input into RESRAD for this scenario, it takes the plutonium 26 years to reach the top of the water table. At this point in time, RESRAD determines instantaneous transport to individuals through ground water, surface water, and fish consumption. Because the plutonium is not water soluble, the

plant uptake mechanism and subsequent dose to individuals via plant intake is less than 5 mrem/yr.

Figure 4.6b shows the excess cancer risk to a population as a result of the radiation doses seen in Figure 4.6a. 26 years after the initial deposition event, the maximum dose rate is 64 mrem/yr.. The 64 mrem will cause an additional 7 cancer deaths in a population of 100,000 persons. These seven deaths which would be attributable to the radiation dose of 64 mrem would be in addition to the 20,000 cancer deaths predicted as the baseline risk for the population (USEPA, 2006).

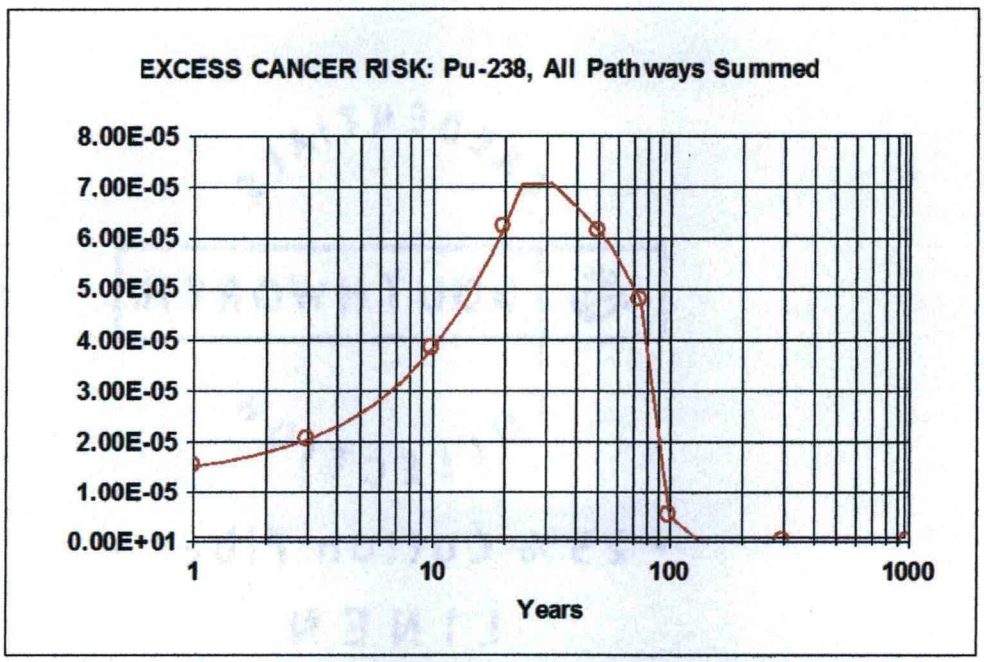

Figure 4.6b Excess cancer risk resulting from living in the deposition zone

6. CONCLUDING REMARKS

Even though the RMFC is a neutron source, it is very unlikely to cause deterministic health effects. The linear no-threshold low dose model, (Cember, 1996) purports that any amount of ionizing radiation increases the likelihood of developing a fatal cancer. Again, from this standpoint the RMFC delivers low dose rates to personnel at a distance from the RMFC or implanted in their body. The resultant dose from ingestion of the RMFC is less than the average annual background radiation received by an average individual in one year's time. The RMFC does produce enough neutrons to deliver a 2.2 rem per year dose rate 30 cm from the device, which is about the same dose rate experienced when one flies on a commercial airplane.

The RMFC is of most concern when the source material is allowed to come in contact with the environs. Of the scenarios examined, only an aerial dispersion event has the ability to deliver high enough acute dose to an organ to cause deterministic health effects.

In order to more accurately model the movement of plutonium through the environment and resultant dose pathways a more detailed analysis of specific hydrology and groundwater flow regimes must be completed.

Safety features can be incorporated into the design of the device to make it more inherently safe. The neutron dose can be limited by enriching both the plutonium oxide, and water in ^{16}O. The radioisotope employed must be manufactured in such a way that atmospheric dispersal of the material as a result of the RMFC being

breached is limited. As the technology moves from its nascent stage and more is learned about the proposed uses of such a device, a more detailed safety analysis can be performed.

REFERENCES

Anderson, M.E. Neutron Energy Spectra of a ^{238}Pu-$^{18}O(\alpha,n)$ Source—Unmoderated and Polyethylene Moderated. Health Physics, Vol. 39, (September), pp. 537-542, 1980.

Anderson, M.E. Neutron Flux, Spectrum, and Dose Equivalent Measurements for a 4500-W(th) $^{238}PuO2$ General Purpose Heat Source, Monsanto Research Corporation, USDOE Contract No. DE-AC04-76-DP00053, 1985.

Arnold, W., Kereiakes, J.G., Bahr, G., Saenger, L., Spickler, J.W. Radiation Dose to Various Organ Sites in a Tissue-equivalent Human Phantom Resulting from Implantation of a Promethium-147 Intracardiac Nuclear Pacemaker. American Journal of Roentgenology, August 1973.

Babut, Bouland, and Fort. Reich-Moore Parameterization of (α,n) Reactions on Light Nuclei: Impact on a Neutron Source Calculation in Oxide Fuel. Commissariat a l'Energie Atomique, 2004.

Berkley Department of Mechanical Engineering (Berkley). Micro Rotary Engine. Available at: www.me.berkeley.edu/mrcl/micro.html—Accessed February, 2006.

Briesmeister, J.F., ed., MCNP: A General Monte Carlo N-Particle Transport Code. Technical Report LA-12625-M, Los Alamos National Laboratory, 1993.

Cember, H. Introduction to Health Physics Third Edition. New York: McGraw-Hill; 1996.

Committee on Airliner Cabin Air Quality (CACAQ). The Airliner Cabin Environment, Air Quality and Safety. National Research Council Commission on Life Sciences. National Academy Press, 1986.

DARPA Radio Isotope Micro Power Program, Nuclear Powered Fuel Cell Project under Air Force Research Lab Award No. FA8651-04-1-0005. August 2004 to June 2006

Environmental Assessment Division at Argonne National Lab (EADANL). RESRAD 6.3. Developed under the joint sponsorship of the United States Department of Energy and the United States Nuclear Regulatory Commission for site-specific dose assessment of residual radioactivity. August, 2005.

From heat sources to heart sources: Los Alamos made material for plutonium powered pumper. Available at: http://www.lanl.gov/source/orgs/nmt/nmtdo/AQarchive/05spring/heart.html—accessed January, 2006.

Furlong, R.R., Wahlquist, E.J. U.S. Space Missions Using Radioisotope Power Systems. Nuclear News, April, 1999.

Garcia-Olivares, A. Resuspension and transport of plutonium in the Palomares area. Journal of Environmental Radioactivity. Vol 37, No 1. 1997.

Green, D., Miller, C., Santavicca, A., Sharp, K. Pulsed Micro Catalytic Combustor for use in a Solid Piston Micro-engine. Proceedings of International Mechanical Engineering Congress and Exposition. November, 2004.

Healy, J.W. A Proposed Interim Standard for Plutonium in Soils. Los Alamos National Lab, Technical Report LA-5483-MS. January 1974.

Homann, S. HOTSPOT version 2.06. Lawrence Livermore National Laboratory National Atmospheric Release Advisory Center. March, 2005.

Hunter, C. H. Savannah River Site Annual Meteorology Report for 2004 (U)" Westinghouse Savannah River Company. Savannah River Site.Aiken, SC 29808. 2004.

International Commission on Radiation Units (ICRU) Report 33: Radiation Quantities and Units. 1980.

International Council on Radiation Protection (ICRP) Publication 21: Data for Protection against Ionizing Radiation from External Sources: Supplement to ICRP Publication 15. New York: Pergamon Press Inc. 1971.

International Council on Radiation Protection (ICRP) Publication 30 Part 1: Limits for Intakes of Radionuclides by Workers. New York; Pergamon Press Inc. 1979

Jacobson, S.A., Epstein, A.H. An Informal Survey of Power MEMS, Gas Turbine Laboratory, Massachusetts Institute of Technology. Available at:http://www.tt-ivanguard.com/montrealreconn/powerMEMS.pdf—Accessed 15 January 2006.

Jannik, G.T., Lee, P.L., Oliver, T.O., Roach, J.L., Jr., and Simpkins A.A. "Risk-Based Radionuclide Derived Concentration Guideline Levels for an Industrial Worker Exposed to Concrete-Slab End States at the Savannah River Site." Westinghouse Savannah River Company. Savannah River Site.Aiken, SC 29808.

Fujiwara, K., Yamana, H., Fujii, T., and Moriyama, H. Solubility product of plutonium hydrous oxide and its ionic strength dependence, *Radiochimica Acta.* **90** (2002) 857-861.

Katholieke Universiteit Leuven (Katholieke). Micro and Precision Engineering Research Group—Microturbine for electric power generation. Available at:www-.mech.kuleuven.be/micro/topics/turbine—Accessed May, 2006.

Knoll, G.F. Radiation Detection and Measurement 3rd Edition. New York: John Wiley & Sons, Inc; 540-545;1999.

Madni, A.M., Wan, L.A. Microelectromechanical systems (MEMS): an overview of currentstate-of-the-art. Institute of Electrical and Electronics Engineers Aerospace Conference Proceedings. March 1998.

Massachusetts Institute of Technology Microsystems Technology Laboratories (MIT). Micro Electric Machines for Micro Turbomachinery. Available at:http://www.mtl.mit.edu/research/annual_reports/2002/02_mems/micro_electric_machines.pdf—Accessed May, 2006

M-DOT Aerospace (MDOT). Micro-Turbines. Available at: www.m-dot.com-/page8.html—Accessed February, 2006.

Misner, Alex. Modeling Radiation and Hydrogen Production in a Radioisotope Micro-Power Source. Thesis for the degree of Master of Science in Nuclear Engineering. Oregon State University, 2005.

NUREG/CR-4214, Rev. 2, Part I, ITRI – 141, Health Effects Models for Nuclear Power Plant Accident Consequence Analysis, October 1993.

Oak Ridge Associated Universities (ORAU), "Plutonium Powered Pacemaker" Health Physics Historical Collection. Available at: http://www.orau.org-/PTP/collection/Miscellaneous/pacemaker.htm—Accessed 15 January 2006.

Scott, B., Peterson, V. Risk Estimates for Deterministic Health Effects of Inhaled Weapons Grade Plutonium. Health Physics, September, 2003.

Simpkins, Ali A. " Routine Dose Estimates For The Removal Of Soil From A Basin To The Burial Ground At The Savannah River Site." Westinghouse Savannah River Company. Aiken, SC 29808. 2001.

Smith, M.L., Greenborg, J., Smith, T.H., Fuqua, P.A. Standards for Prosthetic Devices Containing Radionuclide Power Sources.Medical Research Engineering, Oct-Nov, 1971.

Snyder, W.S., Ford, M.R., Warner, G.G., Fisher, H.L. Estimates of specific absorbed fractions for photon sources uniformly distributed in various organs of a heterogeneous phantom. New York: Society of Nuclear Medicine; MIRD Pamphlet No. 5; 1969.

United State Environmental Protection Agency (USEPA). Understanding Radiation. Available online at http://www.epa.gov/radiation/understand/-health_effects.htm—Accessed April 2006.

United States Environmental Protection Agency Radionuclide Specific Parameters (USEPARSP). Available online at: http://www.epa.gov/superfund/resources/radiation/tbd-part-5-clean.pdf—Accessed December, 2005.

University of Birmingham (Univ. of Birmingham). Micro-Engineering and Nano-Technology: Micro Reciprocating Engine. Available at: www.micro-nano.bham.ac.uk/micro.htm—Accessed February, 2006.

University of Minnesota Department of Mechanical Engineering (Univ. of Minnesota). Micro-Engine Work at the University of Minnesota. Available at: www.menet.umn.edu/~haich/engine—Accessed February, 2006.

Vinson, Deible, and Sindelar. Evaluation of Hydrogen Generation from Radiolysis From Breached Spent Nuclear Fuel. Westinghouse Savannah River Company, 2002.

Vladimirova, M. V., Kulikov, I. A. Formation of H_2 and O_2 in Radiolysis of Water Sorbed on PuO_2. Radiochemistry, Vol. 44, No. 1, 2002; Translated from Radiokhimiya Vol 44, No. 1, 2002.

Vukolov, V.A., Chukreev, F.E. Evaluated (α,n) Reaction Data on Most Important Nuclei Entered in Composition of Chemical Reagents Which used in Nuclear Fuel Work Process. Institute: 4RUSKUR. 1983. Available at: http://www.nndc.bnl.gov/exfor3/exfor00.htm—Accessed October, 2005.

Walther, D.C. and Pisano, A.P. "MEMS Rotary Engine Power System: Project Overview and Recent Research Results. Paper 335, Proc. 4th Intl Symposium on MEMS and Nanotechnology, Charlotte, NC, June 2003, pp. 227-234.

Washington State University News (WSU). WSU Researchers Build World's Smallest Engine, Receive $7 Million Contract. Available at: http://www.wsunews.wsu.edu/detail.asp?StoryID=2873—Accessed February, 2006.

Waters, L.S. ed., MCNPX User's Manual, Version 2.3.0. Technical Report LA-UR-02-2607, Los Alamos National Laboratory, 2002.

Whalen, S., Thompson, M.. Bahr, D., Richards, C., Richards, R. Design, Fabrication and Testing of the P3 Micro Heat Engine. Sensors and Actuators, Vol. 104, No. 3 (2003), pp. 290-298.